Pion-nucleon phase-shift analyses: 0–350 MeV

V. S. Zidell,* R. A. Arndt, and L. D. Roper
Virginia Polytechnic Institute and State University, Blacksburg, Virginia 24061
(Received 20 August 1979)

Energy-dependent and energy-independent partial-wave analyses of the low-energy $\pi^{\pm}p$ elastic and charge-exchange scattering data are presented. Unique, unitary, energy-dependent solutions giving a χ^2/datum of 1 are obtained. The solutions exhibit charge splitting in both the S_{31} and P_{33} partial waves. The T-matrix pole positions and residues of the Δ^{++} and Δ^0 resonances are determined to a new precision. D and F waves are well determined independent of theoretical constraints. New values for the S- and P-wave scattering lengths and effective ranges are reported.

I. INTRODUCTION

Over the last few years a number of experiments have been performed which have considerably improved the precision of the pion-nucleon scattering data (see Table I). These new data have had the effect of making some of the older, widely quoted partial-wave analyses obsolete.[1–3] For this reason we have undertaken a new partial-wave analysis of all the high-precision polarization and total- and differential-cross-section data between 0 and 350 MeV pion laboratory kinetic energy (1078 to 1349 MeV barycentric energy) in order to achieve an energy-dependent representation of the $\pi^{\pm}p$ elastic and charge-exchange scattering data.

Older energy-dependent studies over the same energy range[4,5] have exploited the charge independence of the pion-nucleon interaction within the tolerance of the existing data in order to fit the scattering observables of the different charge states simultaneously. However, as a result of

TABLE I. Pion-nucleon scattering data 0 to 350 MeV since 1971.

ΔE_L (MeV)	Laboratory	Date	Observable	Statistical error (%)	$\chi_D^{2\,a}$	Reference
70–295	CERN	1971	σ_T^0	1	1.85	Bugg *et al.* (T4)
70–295	CERN	1971	$\sigma_T^{\pm}$	0.5	2.1, 3.16[b]	Carter *et al.* (T6)
298–336	LBL	1972	$\sigma_T^{\pm}$	0.4	13.2, 6.6[b]	Davidson *et al.* (T7)
142–272	CERN	1975	$\sigma^0(0°)$	6	2.15	Bayer *et al.* (D7)
207–370	LBL	1972	$\sigma^0(\theta)$	4	3.3	Berardo *et al.* (D8)
21– 96	Saclay	1976	$\sigma^+(\theta)$	2.10	1.04	Bertin *et al.* (D9)
40– 50	LAMPF	1978	$\sigma^+(\theta)$	5	1.23	Blecher (D10)
88–292	CERN	1973	$\sigma^{\pm}(\theta)$	2	2.35, 2.32[b]	Bussey *et al.* (D12)
137–260	LBL	1975	$\sigma^0(\theta)$	7–9	0.17	Comiso *et al.* (D14)
23– 43	Saclay	1973	$\sigma^0(180°)$	10	0.03	Duclos *et al.* (D19)
277–334	LNPI	1976	$\sigma^{\pm}(\theta)$	2.5	1.71, 7.38[b]	Gordeev *et al.* (D32)
147–347	PPA	1971	$\sigma^0(\theta)$	3–6	3.39	Hauser *et al.* (D34)
114–227	CERN	1974	$\sigma^0(160°)$	4–14	0.01	Jenefsky *et al.* (D36)
292–308	SIN	1978	$P^-(\theta)$	7–16	1.05	Alder *et al.* (P1)
236	SIN	1975	$P^+(\theta)$	10–30	0.65	Amsler *et al.* (P2)
95–194	SIN	1976	$P^+(\theta)$	5–30	1.08	Amsler *et al.* (P3)
291–310	SIN	1977	$P^+(\theta)$	10–20	0.72	Dubal *et al.* (P6)
243–349	LBL	1973	$P^{\pm}(\theta)$	10–15	2.22, 2.14[b]	Gorn (P9)

[a] χ_D^2 is the χ^2 per data point for a given data set and includes the normalization χ^2.
[b] The first number corresponds to π^+p and the second to π^-p.

the high precision of recent total- and differential-cross-section measurements (see Refs. T6, T7, D9, D10, D12, D19, and D32 in Appendix A), recent phase-shift analyses[2,3] have permitted overt violations of isospin conservation in the pion-nucleon amplitudes. In particular, Carter, Bugg, and Carter[2] allowed for charge splitting in the P_{33} partial wave, arising mainly from the Δ^{++}-Δ^0 mass difference, by determining the P_{33} phase shift in π^+p scattering independently of its value in π^-p scattering. Our results also indicate that it is not possible to obtain a good fit to all the pion-nucleon scattering reactions using isospin-conserving amplitudes. In this analysis, charge splitting has been taken into account in both the S_{31} and P_{33} partial waves by allowing the P_{33} phase shift and the S_{31} scattering length to adopt different values in π^+p and π^-p scattering.

For the π^+p system we have obtained a unique, parametrization-independent set of phase shifts yielding a χ^2 per data point of 1.43. This solution is highly stable to data pruning and results in a reliable determination of the S-, P-, and D-wave phase shifts. We emphasize that these are not the phases that would necessarily be obtained from a π^-p data analysis.

It is usual, assuming charge independence of the pion-nucleon interaction, to use the resulting phase shifts as input in a partial-wave analysis of the π^-p scattering data. It is our experience that it is not possible to achieve a purely charge-independent partial-wave representation of the low-energy data without explicitly incorporating complicated, model-dependent Coulomb corrections. Charge splitting is best allowed for in both the S_{31} and P_{33} partial waves. Apart from this assumption it is not possible to obtain a unique π^-p scattering solution. The other $I=\frac{3}{2}$ waves have been taken directly from the π^+p analysis.

For the π^-p system our basic fit to all the data gives a χ^2 per data point of 2.08. The elimination of sufficient data to give a 50% confidence level exhibited no important change in the values of the phase shifts. The solution is largely parametrization independent and leads to precise values for the S, P, and D waves.

We have also performed energy-independent analyses at several selected energies as a check on the uniqueness of the energy-dependent representation, as an aid in elucidating inconsistencies, and as a tool for checking the validity of the errors obtained from the error matrix. No significant discrepancies between the energy-dependent and energy-independent solutions are found.

In Sec. II we discuss the data base used in our analysis. It essentially consists of the most recent and most precise pion-nucleon scattering data available, supplemented by reliable older data in energy regions where new data have not been taken.

In Sec. III we outline the coupled-channel K-matrix formalism on which our phenomenological fits are based. The goal of an analysis of this kind is to make use of a minimum of theoretical assumptions in order to achieve as simple and accurate a representation of the data as possible. This should be of considerable use to the modelist since the complications of fitting and renormalizing large quantities of scattering data have been eliminated. To this end no attempt was made to include all the effects of the Coulomb interaction. The phase shifts reported in this paper are the so-called "nuclear" phase shifts which are obtained when a partial-wave analysis is carried out after corrections for the Coulomb amplitude and Coulomb-nuclear interference are made.

To simplify the problem, the following assumptions were made:

(1) Only partial waves up to $l=3$ are assumed to contribute to the scattering.

(2) Pion and nucleon isospin-multiplet mass differences are neglected, and thus the small difference in phase space available for π^-p and charge-exchange scattering is neglected.

(3) We assume the inelastic scattering is due solely to the channel $\pi^-p \to \pi\Delta$ in the P_{11} state.

(4) We assume that contributions from the radiative-capture process are negligible.

In the context of these assumptions, our formalism satisfies unitarity, has the proper elastic and inelastic threshold behavior, and is continuable into the complex energy plane.

The pion-nucleon phase shifts obtained from our analyses are reported in Sec. IV. We regard these phases as the best representation of the available data made to date. The S and P waves possess very small errors and are insensitive to the analytical representation of the amplitude. Both the magnitude and signs of the D and F waves are well determined by the energy-dependent fit. We also include the results of a corresponding energy-band analysis. Fits are displayed to some of the most recent differential-cross-section and polarization data, and the results of this analysis are compared with the energy-independent analyses of Ayed[6] and the SIN group (P1, P2, P3, and P6). Preliminary results on the π^+p system have been reported earlier.[7]

In Sec. V, an elastic resonance parametrization similar to that employed by Lichtenberg[8] is used to obtain new values for the T-matrix pole positions of the Δ resonances. We find $M_{++}=1210.4 \pm 0.7$ and $\Gamma_{++}=99.49\pm 0.28$ MeV independent of ef-

fects of the Coulomb barrier, the form of the phase-space factor, and of the background parametrization. An analogous determination of the Δ^0 pole was also made, yielding $M_0 = 1210.3 \pm 0.36$ and $\Gamma_0 = 108.0 \pm 0.52$ MeV. A precise determination of the Δ residues and background is also discussed.

In Sec. VI we present our predictions for the low-energy spin-rotation parameters, differential cross sections, and polarization in regions of experimental interest. This paper will form the core for future partial-wave analyses at higher energies in anticipation of new measurements to be performed using high-intensity pion beams at SIN, TRIUMF, and LAMPF.

II. PION-NUCLEON DATA BASE

The data base for the πN scattering reaction consists of a collection of the most precise measurements of the πN total cross sections σ_T, differential cross sections $\sigma(\theta)$, and recoil-proton polarizations $P(\theta)$, measured in the energy range 0 to 350 MeV. Superscripts +, −, and 0 will be used to denote π^+p, π^-p elastic, and π^-p charge-exchange reactions, respectively. Throughout the following, all energies will be quoted as laboratory-frame pion kinetic energies unless otherwise indicated. The energy cutoff in this analysis, 350 MeV, was chosen so as to include only those effects arising in the first, or P_{33}, resonance region.

As a further constraint on the values of the phase shifts calculated from our partial-wave analyses we have included as theoretical input selected values of the real part of the forward elastic scattering amplitude, $\mathrm{Re}f^{\pm}(0)$, as computed by Carter and Carter.[9] This quantity is dependent on theory-laden values for the pion-nucleon coupling constant, the S-wave scattering lengths (which the authors obtained from their own low-energy data analyses), and on experimental values for the total cross sections. The values for $\mathrm{Re}f^{\pm}(0)$ we have included in our data base occur in steps of 10 MeV/c and possess errors of about 5% at low energies and 1% at high energies. We have checked the sensitivity of our values for the phase shifts on different theoretical calculations of $\mathrm{Re}f^{\pm}(0)$, including the recent work of Englemann and Hendrick.[10] Only irrelevant changes occur.

Since the last analysis of the pion-nucleon scattering data by our group in 1965,[4,5] the data have improved substantially in both quality and quantity. Appendix A contains a complete listing of our data base. The starting point for this study was the CERN 1973 compilation.[11] We excluded a fair amount of pre-1967 data pre-empted by recent higher-precision measurements and included a number of recent experiments not covered by CERN 1973 (see Table I).

Our pion-nucleon data base consists of 1572 data points (835 for π^+p and 737 for π^-p). The data breakdown is illustrated in Figs. 1(a)–1(c), where the division into data types at specific energies and over specific angular ranges is given. In Table I we list the most recent additions.

A. π^+p elastic data

Complete references to the pion-nucleon data used in this analysis are contained in Appendix A. To avoid redundancy only values of σ_T that are not integrations of $\sigma(\theta)$ at the same energy are used. Especially notable are the precise measurements of $\sigma_T^{\pm}$ by Carter *et al.* (T6). Further precision measurements of $\sigma_T^{\pm}$ are presently underway at SIN.[12]

The $\sigma^+(\theta)$ data are spread fairly uniformly over the entire energy range, though they stop abruptly below 20 MeV due to unresolvable background problems. Overall, these data possess errors on the order of 4% or less. The quality of the data below 100 MeV has been generally improved by the measurements of Bertin *et al.* (D9) giving precise $\sigma^+(\theta)$ values at seven energies below 100 MeV. (The measurements at 67.4 MeV, however, were not consistent with our solution or with nearby data and were excluded prior to the analysis.) The $\sigma^+(\theta)$ data cover the angular range 30°–160° quite completely; there are few measurements below 30° due to Coulomb interference. The low-energy data have recently been supplemented by precision measurements of $\sigma^+(\theta)$ at 39.8 and 49.9 MeV by Blecher *et al.* (D10). In addition, higher-energy data have been reported by Gordeev *et al.* (D32). The total cross sections calculated from this experiment are in better agreement with the data of Davidson *et al.* (T7) than Carter *et al.* (T3).

Considered as a whole, the π^+p polarization data are in fair shape. These data are very important as the unpolarized differential-cross-section measurements at high energies are insensitive to D waves, which may be determined by precise measurements of $P(\theta)$. Furthermore, measurements of $P(\theta)$ depend on interference between different partial waves and thus yield information on the nonresonant phases. The recent development of intense pion beams has permitted the $P^+(\theta)$ data to be measured at much lower energies than were formerly available. Amsler *et al.* (P2 and P3) have recently reported measurements of $P^+(\theta)$ at six energies between 94 and 237 MeV. Generally speaking, the polarization data are concentrated in the backward direction and often pos-

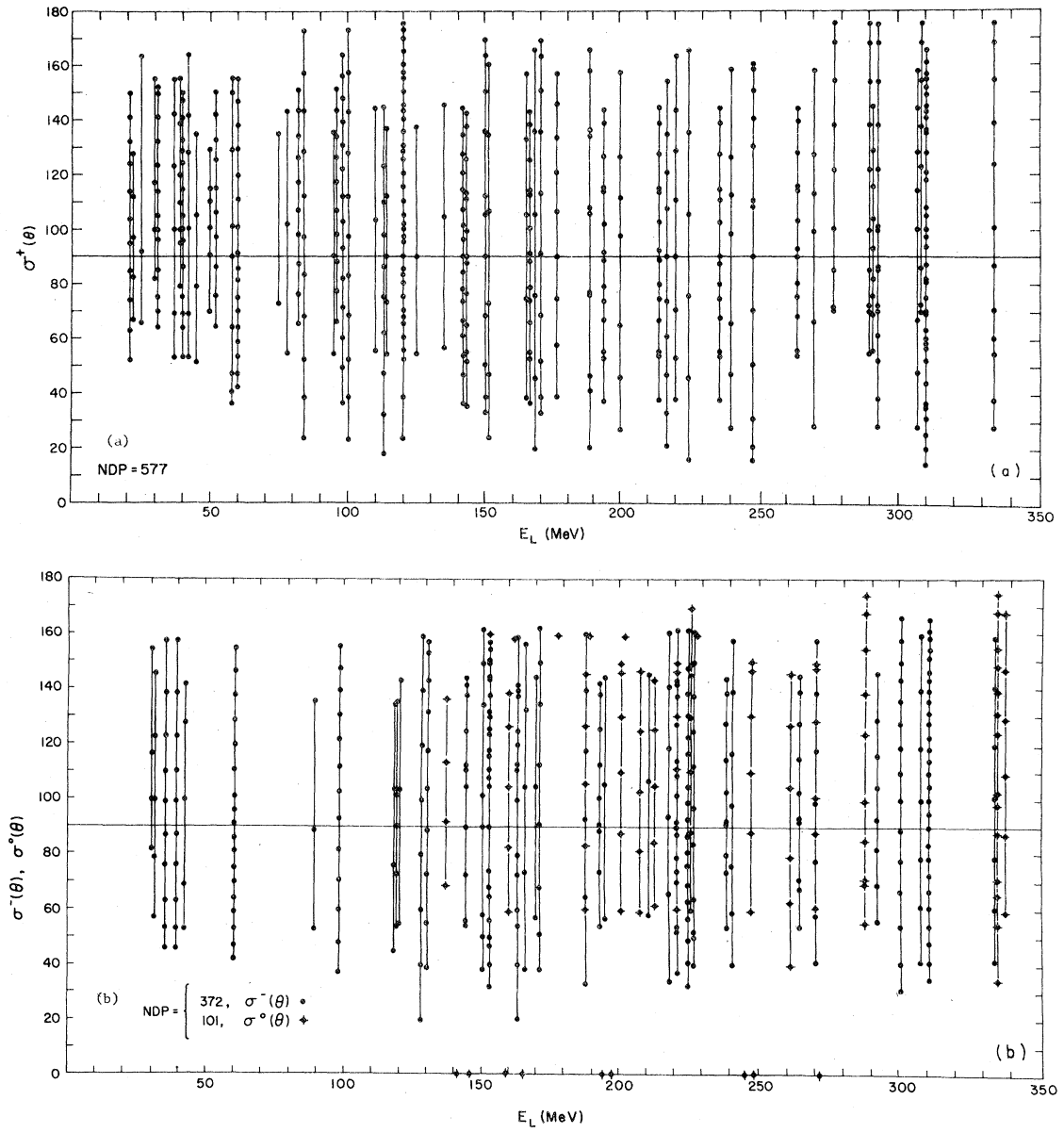

FIG. 1. Data used in the analyses. (a) $\pi^+p \to \pi^+p$ differential cross sections. (b) $\pi^-p \to \pi^-p$ and $\pi^-p \to \pi^0n$ differential cross sections. (c) Polarization and total cross sections. NDP = number of data points.

sess very large errors, especially where their absolute value is small.

B. π^-p elastic data

Discrepancies between measurements of σ_T^- performed at different laboratories still persist. The high-energy Carter *et al.* σ_T^- data (T6) are not consistent with older measurements or with the more recent precise measurements by Davidson *et al.* (T7). As a result we were obliged to eliminate the Davidson *et al.* measurements at 298 and 336.1 MeV in our preliminary analysis.

The π^-p differential-cross-section data base does not possess the quality characteristic of the $\sigma^+(\theta)$ data base. It lacks both a comprehensive energy distribution and uniform angular coverage. The only new measurements are those of Bussey *et al.* (D12) and Gordeev *et al.* (D32). We found it necessary to discard the π^-p elastic differential-cross-section measurements of Bussey *et al.* at 88.5 MeV due to its large contribution to χ^2. The total cross sections calculated from the Gordeev *et al.* data are known to be in systematic 10% dis-

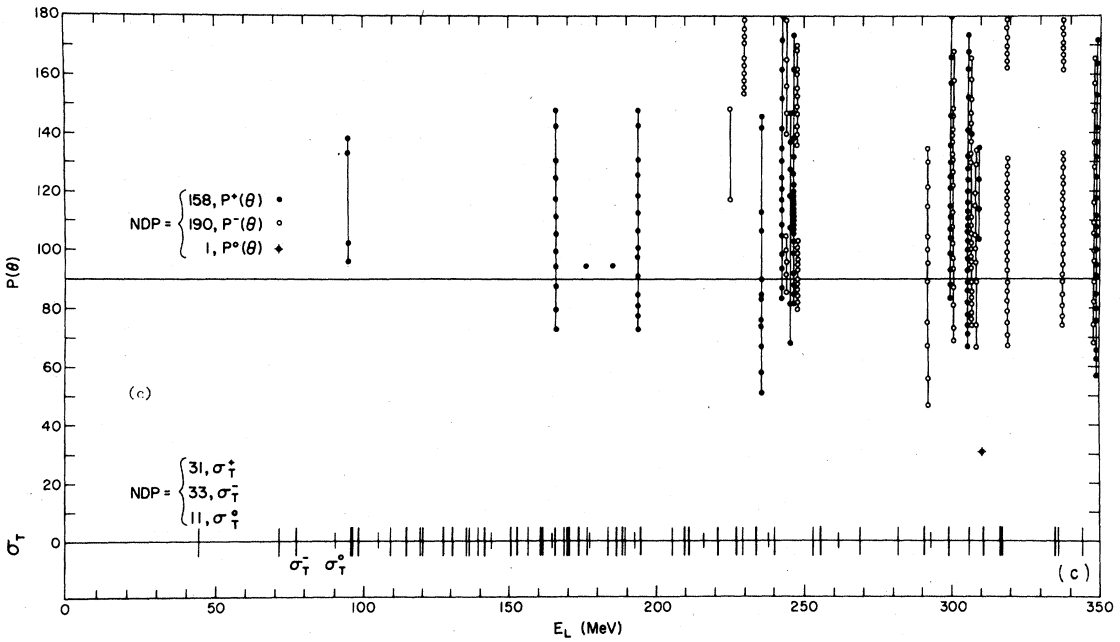

FIG. 1. (*Continued*)

agreement with previous σ_T^- data. [Measurements of $\sigma^{\pm}(\theta)$ for pion energies of 300–580 MeV are planned at LAMPF.[13]]

The situation with the $\pi^- p$ polarization data is less satisfactory than in the $\pi^+ p$ case. There exist only a few measurements over a limited energy range, the most recent being those of Alder *et al.* (P1) at 291.5 and 308 MeV. These measurements yield an improved determination of the S_{11} partial wave.

C. Charge-exchange data

For this reaction, with the exception of one polarization datum P^0 ($E_L = 310$, $\theta = 180°$), only the angular distributions and total cross sections have been measured. Charge-exchange scattering is difficult to measure, but is very important in determining the small $I = \frac{1}{2}$ component and in resolving the apparent violation of the triangle inequalities due to I-spin breaking. Many new measurements have been performed in response to these needs (see Table I) and new high precision measurements of $\sigma^0(\theta)$ and $P^0(\theta)$ between 147 and 500 MeV are underway at LAMPF.[14] Because the low-energy Bugg *et al.* σ_T^0 data (T4) are not consistent with earlier measurements, but are of high precision, we use it as our sole source of knowledge on σ_T^0. These data are not only important in aiding in a determination of the Δ^{++}-Δ^0 mass splitting but tend to pin down P_{13} by interference with P_{33}. As can be seen from an examination of Fig. 1(b), there is a paucity of good charge-exchange data, especially at low energies and small angles.

Both the $\pi^- p$ elastic and charge-exchange differential-cross-section data are concentrated at somewhat larger angles than the $\sigma^+(\theta)$ data. This may be significant since the πN data are uncorrected for errors due to external soft-photon emission accompanying the hadronic scattering. Calculations by Sogard[15] and Borie[16] indicate that the fractional change in the measured cross section due to external bremmstrahlung is a t-dependent correction and may be as large as 4% at 350 MeV in the backward scattering region (about 1% in charge-exchange scattering). All calculations of soft-photon emission are, of course, dependent on the energy resolution of the experiment. The percentage increases rapidly as the energy resolution decreases. In $\pi^+ p$ scattering, on the other hand, the fractional change in the measured cross section due to bremmstrahlung is at most only 1% for a typical energy resolution of 10%. Radiative corrections are not significant for the polarization data.

Measurements of internal bremmstrahlung in πN scattering, i.e., photon emission from the strongly interacting intermediate state, have been conducted by Sober *et al.*[17] in the hope of investigating the electromagnetic properties of the Δ resonance and off-mass-shell πN amplitudes. This process contributes less than 0.1 mb at 294 MeV and may be safely neglected.

Finally, the radiative-capture reaction $\pi^- p \to \gamma n$

is entirely negligible at the energies at which our data exist, contributing only about 1 mb to the total cross section at the Δ resonance. Only at low energies, near the elastic threshold, is $\sigma_T(\pi^- p \to \gamma n)$ comparable to σ_T^0.

III. PHASE-SHIFT PARAMETRIZATIONS

The pion and the nucleon scatter through both the strong and electromagnetic interactions. In this paper we are interested only in the "nuclear" phase shifts which result when one eliminates only the effects of the electromagnetic interactions due to single-photon exchange between a point pion and a point nucleon. Thus the so-called inner Coulomb corrections arising from extended pion and proton charge distribution are not included, nor are the effects of vacuum polarization or bremmstrahlung. Likewise, the indirect electromagnetic effects which arise, for example, from the nucleon mass difference, radiative correction to the pion-nucleon vertices, etc., are not included. Furthermore, once electromagnetic corrections to first order in α are considered, it is necessary to take account of the competing photon-nucleon channel. All these effects are either negligible or contribute to the total phase shift an amount which cannot be calculated without presuming a specific model for the strong interaction—a model, moreover, which must be consistent with the results of a partial-wave analysis itself. However, it is precisely the absence of an acceptable model for the strong interactions that makes a phase-shift analysis necessary in the first place. There is no consensus as to the correct way to make these corrections, and, in our judgment, a model-independent analysis of the scattering data mandates the necessity of reporting the nuclear rather than the hadronic (or "strictly nuclear") phase shifts.

In order to incorporate unitarity for the electromagnetic and strong interactions separately we assume that the product S matrix

$$S = S_C S_N \tag{1}$$

describes the composite interaction correctly. Here S is the observed S-matrix element, S_C is the S-matrix element describing πN scattering purely through the electromagnetic (or Coulomb) interaction, and S_N is the nuclear S-matrix element. From Eq. (1) it follows that the T-matrix element can be written as

$$T = S_C T_N + T_C . \tag{2}$$

A convenient way to parametrize the amplitudes and to describe threshold effects is to write the nuclear T matrix in terms of the K matrix as follows:

$$T_N = K(1 - iK)^{-1} . \tag{3}$$

The K matrix is real and symmetric as required by unitarity and time-reversal invariance. We may explicitly remove the threshold phase-space factor from K by introducing the reduced K matrix $\overline{K}$ by

$$K = \rho^{1/2} \overline{K} \rho^{1/2} , \tag{4}$$

where ρ is the diagonal phase-space matrix involving the barycentric momenta of the various channels.

The great utility of the K-matrix formalism is that it provides a neat phenomenological means of describing a multichannel scattering process in which partial-wave unitarity and S-matrix analyticity may easily be incorporated. Furthermore, the scattering amplitudes may be parametrized by simple analytic expressions which may be conveniently constructed to satisfy the correct threshold behavior for the elastic and inelastic channels and which can be analytically continued into the multisheeted complex energy plane in order to locate the relevant S-matrix singularities.

The K-matrix method is most useful, however, only in the case of two-body final states. Fortunately, the $\pi\pi N$ mass spectra[18] suggest that above the pion production threshold $W_\pi = 1217.4$ MeV the $\pi N \to \pi\pi N$ reaction is dominated by isobar production. Thus the K matrix formalism is applicable,[19] and we are led to consider the following two-body and pseudo–two-body channels (W_i denotes the threshold barycentric energy of the ith channel):

channel 1: $\pi^- p \to \pi N$, $W_1 = 1078$ MeV,

channel 2: $\pi^- p \to \pi \Delta$, $W_2 = 1350 \pm 120$ MeV,

channel 3: $\pi^- p \to \epsilon n$, $W_3 = 1638 \pm 600$ MeV.

Here ϵ represents the very broad $I = 0$ S-wave pion-pion resonance. The photoproduction channel $\pi^- p \to \gamma n$ is not included because it is negligible at these energies, contributing at most only 0.1 mb (Ref. 20).

Thus, the whole πN scattering process may be described by the 2×2 K matrix

$$\overline{K} = \begin{pmatrix} \overline{K}_{11} & \overline{K}_{12} \\ \overline{K}_{12} & \overline{K}_{22} \end{pmatrix} , \tag{5}$$

where

$$\begin{aligned} &\overline{K}_{11} = \pi N \to \pi N \text{ amplitude} , \\ &\overline{K}_{12} = \pi N \to \pi \Delta \text{ (or } \pi N \to \epsilon N \text{) amplitude} , \\ &\overline{K}_{22} = \pi \Delta \to \pi \Delta \text{ (or } \epsilon N \to \epsilon N \text{) amplitude} , \end{aligned} \tag{6}$$

and where the total and orbital angular momenta as well as the isospin indices have been suppressed. The elastic element of the T matrix may now be written as

$$T_{11}=K'(1-iK')^{-1}, \tag{7}$$

where

$$K'=\rho_1[\overline{K}_{11}+i\rho_2\overline{K}_{12}^{\,2}(1-i\rho\overline{K}_{22})^{-1}]. \tag{8}$$

The amplitudes are normalized so that

$$\sigma_{ij}=4\pi\lambda\!\!\!^{-2}\,|T_{ij}|^2, \tag{9}$$

where $\lambda\!\!\!^{-}=\hbar/q$, and q = barycentric momentum.

Guided by the $\pi\pi N$ analyses,[18] which indicate that inelastic contributions to π^+p scattering are negligible and that inelasticity in all partial waves other than the P_{11} may be ignored, we are led to some significant simplifications. For all the elastic waves, the K matrix is related to the phase shift by

$$K=\tan\delta, \tag{10}$$

and for the P_{11} a two-channel $(\pi N, \pi\Delta)$ or $(\pi N, \epsilon N)$ representation is sufficient for a complete description of the scattering data in the energy range of interest.

The elements of the reduced K matrix may be parametrized as analytic functions of the pion lab kinetic energy[21] E_L in any way that preserves the reality and symmetry of the K matrix and that incorporates the q^{2l+1} threshold behavior for a channel with orbital angular momentum l. A variety of such parametrizations have been used in our analysis, including

elastic resonance (form 1) (see Sec. V),

effective range (form 2)

$$\overline{K}_{11}=\left[\sum_{n=1}^{5}P_n(E_L/1000)^{n-1}\right]^{-1}, \tag{11}$$

polynomial (form 3)

$$\overline{K}_{11}=\sum_{n=1}^{5}P_n(E_L/1000)^{n-1}.$$

Here P_n represents a free phenomenological parameter (labeled by l, J, and I) which must be determined by the least-squares fit. The polynomial parametrization cannot accommodate a resonant phase because $\tan\delta$ cannot have a pole. This limitation is circumvented by either an elastic resonance formula or by use of the effective-range parametrization, which is also very useful for the determination of scattering lengths and effective ranges. Its disadvantage is that it does not permit a phase that changes sign. In all these parametrizations we neglect contributions to $\overline{K}$ from the closed channel described by $\overline{K}_{22}$ and approximate the mixing channel by a positive constant (to satisfy unitarity) for the P_{11} state

$$\overline{K}_{12}=P_6^{\,2}. \tag{12}$$

Equations (3)–(12) completely determine the unitary, nuclear T-matrix amplitude T_N. In practice, a single-channel parametrization is sufficient for all but the P_{11} partial wave. All other S and P waves may be described by three or four variable parameters and the D and F waves by one or two parameters.

This formalism does not explicitly assume the validity of any specific model. It does not involve complicated integral or differential equations and thus is especially useful in energy-dependent partial-wave analyses by computer. It does constitute a model in the weak sense that an *a priori* analytic structure is imposed on the amplitudes; a structure in which all singularities other than the elastic threshold and P_{33} pole (and $\pi\Delta$ threshold for P_{11}) are ignored. The other relevant singularities (left-hand cut, inelastic thresholds except for P_{11}, higher resonances, etc.) are unimportant in the limited energy range considered here.

Form dependence also enters into a consideration of the phase-space matrix ρ. For the elastic channel we take

$$(\rho_1)_l=[q(W,\mu,M)]^{2l+1}, \tag{13}$$

where μ is the pion rest mass, M is the nucleon rest mass, and $q(W,m_1,m_2)$ is the relativistic barycentric momentum for two particles with masses m_1 and m_2 and total barycentric energy W:

$$q^2(W,m_1,m_2)=\frac{1}{4W^2}[W^2-(m_1+m_2)^2][W^2-(m_1-m_2)^2]. \tag{14}$$

For the inelastic channel, the threshold behavior has been modified to include the effects of instability in the final state. We have assumed that the unstable particle mass is smeared out in accordance with a Gaussian distribution and have adopted the integral form

$$(\rho_2)_l=\frac{1}{\Gamma_u\sqrt{\pi}}\int_{M_c}^{\infty}dm'[q(W,m_s,m']^{2l+1}\times\exp[-(m'-m_u)^2/\Gamma_u^{\,2}], \tag{15}$$

where l is here the lowest orbital angular momentum of the final-state coupling to a given partial wave (the P_{11} couples to the $\pi\Delta$ P wave and the ϵN S wave). In this expression m_u is the mass and Γ_u the width of the unstable state. The normalization is chosen so that in the stable-particle limit

$$(\rho_2)_l \xrightarrow[\Gamma_u \to 0]{} [q(W, m_s, m_u)]^{2l+1}, \tag{16}$$

as required. The lower limit of integration was chosen to ensure the absolute closing of the inelastic channel at and below the pion-production threshold ($M_c = \mu + M$ for $\pi\Delta$ and $M_c = 2\mu$ for ϵN). Proper threshold behavior is obtained through the first term in brackets in Eq. (14). The other factors in the expression for q^2 were replaced by nonrelativistic approximations in order to do away with uninterpretable singularity structure and to facilitate the integration in Eq. (15). These modifications preserve the proper threshold behavior, which is the only important aspect of phase space for these calculations. The form of q^2 actually used in the representations is given by

$$\rho_l = \{\tfrac{1}{1000}[W^2 - (\mu + M)^2]^{1/2}\}^{2l+1}. \tag{17}$$

Ideally we would prefer to use an exact relativistic form for the Coulomb T-matrix element T_C in order to guarantee unitarity, but in the absence of this we use an approximate amplitude which is relativistically correct to first order in $\alpha = e^2/\hbar c$ and correct to all orders of α nonrelativistically. This is accomplished by adding the full nonrelativistic Coulomb amplitude to the single-photon-exchange amplitude, suitably corrected for double counting. Considerable work has recently been done on the construction of full relativistic amplitudes for πN electromagnetic scattering,[22] though in our energy range the refinements prove to be of little consequence (see Appendix B).

The Coulomb S matrix S_C may be written in terms of the Coulomb phase shifts σ_l as

$$S_C = \exp(2i\sigma_l), \tag{18}$$

where

$$\sigma_l = \arg\Gamma(l + 1 + i\eta). \tag{19}$$

Equation (19) involves the model-dependent Coulomb parameter η. For nonrelativistic scattering it has the form

$$\eta = \alpha(M_r/p_L), \tag{20}$$

where M_r is the reduced mass of the pion-nucleon system, and p_L is the laboratory momentum of the incident pion. A variety of two-particle relativistic wave equations employing a Coulomb potential interaction can be shown to yield values for η between its nonrelativistic value in Eq. (20) and its relativistic value

$$\eta = \alpha \frac{\mu + E_L}{[E_L(E_L + 2_u)]^{1/2}}, \tag{21}$$

which results from solving the Klein-Gordon equation with a Coulomb potential in the static nucleon limit.

For technical consistency, the energy-dependent representations given in Eq. (8) must be altered to include low-energy charge effects due to the penetration of the proton Coulomb barrier by the pion. For the coupled-channel case, nonrelativistic scattering theory gives[23]

$$\mathrm{Re}K' = \rho_1 \bar{K}_{11}\{1 - [2\eta h(\eta^2)/C_0^2]\rho_1 \bar{K}_{11}\}^{-1}, \tag{22}$$

$$\mathrm{Im}K' = C_{l1}^2 \rho_1 \bar{K}_{12}^2 C_{l2}^2 \rho_2, \tag{23}$$

where C_l^2 are the Coulomb-barrier-penetration factors,

$$C_0^2 = 2\pi\eta/[\exp(2\pi\eta) - 1], \tag{24}$$

$$C_l^2(\eta) = C_{l-1}^2(\eta)[1 + (\eta^2/l^2)], \quad \text{for } l \neq 0 \tag{25}$$

and

$$h(\eta^2) = \eta^2 \sum_{r=1}^{\infty} \frac{1}{r(\eta^2 + r^2)} - \ln|\eta| - \gamma, \tag{26}$$

where $\gamma = 0.577\,16$ is Euler's constant. It turns out that the removal of the Coulomb-barrier factors leads to virtually no change in the phase shifts obtained from our analyses. There is also no significant dependence on the form of the Coulomb parameter η. Thus the modifications required by Eqs. (22) and (23) are actually not essential, given the present precision of the πN scattering data.

The nuclear amplitudes defined by Eq. (3) must be distinguished from the pure hadronic, isospin-invariant amplitude T_H, which would presumably result if the pion and nucleon interacted only through the strong interaction. In this case, the amplitudes for $\pi^+ p$ elastic and $\pi^- p$ charge-exchange scattering, T_H^+ and T_H^0, respectively, could be written as linear combinations of the pure isospin amplitudes T_1 and T_3, describing scattering in the $I = \frac{1}{2}$ and $I = \frac{3}{2}$ states.

Former partial-wave analyses were able to utilize the relations

$$\begin{aligned} T_N^+ &= T_3, \\ T_N^- &= (T_3 + 2T_1)/3, \\ T_N^0 &= \sqrt{2}\,(T_3 - T_1)/3. \end{aligned} \tag{27}$$

applied to the nuclear amplitude in order to analyze $\pi^+ p$ and $\pi^- p$ scattering data simultaneously. What made this permissible were the large errors on the cross-section measurements, which precluded the possibility of distinguishing the corrections due to different charge states. Random and systematic errors on recent cross-section measurements are now so small that errors resulting from the neglect of full Coulomb corrections are ponderable and as a result it is not

possible to fit π^+p and π^-p data simultaneously using Eq. (27). Strictly speaking, the Coulomb potential is off-diagonal in an I-spin representation because it acts only between π^-p states. As a result, Eq. (27) may be modified to include an isospin-mixing amplitude between $I=\frac{1}{2}$ and $I=\frac{3}{2}$ states. This complication is not explicitly included in our analysis.

Since the $I=\frac{3}{2}$ partial waves are best determined by the π^+p data, in our analyses charge splitting is included phenomenologically by fitting the π^+p data separately from the π^-p data. The resulting $I=\frac{3}{2}$ phases are then used in the analysis of the π^-p scattering data to model the $I=\frac{3}{2}$ component, after permitting charge splitting in the P_{33} phase shift and the S_{31} scattering length. This choice deserves some further explanation.

First, if no charge splitting at all is permitted it is not possible to find an acceptable set of $I=\frac{1}{2}$ phases to describe the π^-p data no matter how many parameters are used. The reverse procedure of first allowing the π^-p data to determine values for the $I=\frac{3}{2}$ phases shifts is equally ineffective. Conversely, if charge splitting is permitted in all $I=\frac{3}{2}$ partial waves we obtain a multiplicity of solutions for the $I=\frac{1}{2}$ component, all of equal statistical quality, all differing in the signs and magnitudes of the peripheral waves and in the structure of the S_{11}. This ambiguity in the π^-p solution arises from the small magnitude of the $I=\frac{1}{2}$ component compared to the $I=\frac{3}{2}$ component, a difficulty accentuated by the large errors on the charge-exchange data.

A unique solution can be obtained, however, if the parametrization is sufficiently constrained by allowing charge splitting in only some of the partial waves. *A priori*, we do not anticipate significant charge splitting in the D or F waves. The mass difference between different charge states of the Δ is expected to give rise to significant charge splitting in the P_{33}. Whether the S wave also participates is basically a matter for the data analysis to reveal.

A three-step procedure was used to choose the best phase-shift solution. First, the π^+p data were fitted and the parametrization optimized to obtain the best fit using a minimum number of parameters. Second, these $I=\frac{3}{2}$ parameters were fixed at the values found and used in the analysis of the π^-p data. The $I=\frac{1}{2}$ parameters were varied to optimize the solution. Finally, charge splitting was introduced in different partial waves until a new optimum solution was established. P_{33} splitting alone gave $\chi_D^2=2.31$. When the S_{31} scattering length parameter was allowed to vary as well, we obtained $\chi_D^2=2.08$. Permitting charge splitting in all $I=\frac{3}{2}$ partial waves gave only a slightly smaller χ_D^2 of 2. Because of the large effect of the S_{31} scattering length, we feel charge splitting in both the P_{33} and the S_{31} is justified.

Further support for this conclusion comes from the results of an energy-indepndent phase-shift analysis of the data in the second resonance region (300 to 600 MeV). Laurikainen and Tornqvist[24] found "anomalously large" isospin breaking in S_{31}, and a more repulsive force in the neutral charge state than in π^+p. A comparison of the scattering lengths obtained from our fits (see the discussion in Sec. VII) is consistent with their conclusion.

It is important to note at this point the purely experimental sources of apparent I-spin breaking. These include, first of all, systematic errors in cross-section measurements. This was the explanation of the apparent I-spin-nonconserving amplitude in π^-p backward scattering reported a few years ago.[25] Secondly, as pointed out by Sogard,[15] the neglect of external bremmstrahlung corrections may strongly affect the I-spin relations.

IV. πN SOLUTIONS

The results of our phase-shift analyses are a set of phenomenological parameters P_n occurring in Eqs. (11) and (12), which minimize the total χ^2. The χ^2 and the full error matrix derived from it have been defined and discussed elsewhere.[26] Normalization parameters λ are included in $\sigma(\theta)$ and $P(\theta)$ measurements at fixed energies and variable angles as multiplicative factors of the predicted values of the observable. The equations relating the phase shifts to the observables are given in Appendix B.

Initial sets of phase parameters were determined by performing numerous random starts. The minimization procedure consists of both grid and matrix search algorithms. The details have been presented elsewhere.[27] The statistical quality of a solution is measured by χ_D^2, the χ^2 per data point. What we term the basic fit constitutes the best fit to all the data contained in our data base. For the π^+p system, the basic fit gives a $\chi_D^2=1.43$, and for the π^-p system we obtain $\chi_D^2=2.08$. These χ^2 values are obtained by simultaneously renormalizing all the angular data (variable λ for each experiment) during the minimization, a procedure that contributes a normalization χ^2 of 64 to the total sum of approximately 1172 for π^+p and 75 to the total of 1536 for π^-p. For purposes of comparison, we obtain a measure of the internal inconsistency of the data by fixing $\lambda=1$. The unrenormalized χ_D^2 are 2.0 and 5.0 for

π^+p and π^-p, respectively.

The πN solutions we obtain are unique and parametrization independent, i.e., we find the resulting phase shifts are virtually identical when represented by any of the equations in (11). In view of the stability of these phases to the elimination of high χ^2 data and their form independence, we prefer to focus our attention mainly on the reduced data base and the pruned solutions.

We label our solutions as follows: A0 and B0 refer to the basic fits (to all the data) for π^+p and π^-p scattering, respectively. A1 denotes the pruned solution which results when the P_{33} is described by a Lichtenberg T-matrix pole formula (see Sec. V) and all other phases are parametrized by a polynomial or inverse polynomial in E_L. A2 denotes the pruned solution resulting from an effective range (or form 2) parametrization of all the phases, and A3 denotes the pruned solution we obtain when all the partial waves except P_{33} are represented by a polynomial in E_L (form 3). Solutions B1, B2, and B3 are the π^-p pruned solutions defined in a similar way. From time to time we shall refer to the solution collectively as solutions A (or B). All pruned solutions give $\chi_D^2 = 1.0$. Other relevant statistical information is presented in Tables II and III.

There are often sources of systematic error not taken into account or underestimated by the experimentalists. We have checked the sensitivity of the fit to the normalization errors (typically on the order of 5%) by floating them, that is, we set $\Delta\lambda = 100\%$. Then χ_D^2 drops to 1.36 for π^+p with no significant change in the values of the phases. For the π^-p system, on the other hand, χ_D^2 drops to 1.85, and the phase shifts adopt the same structure with significantly different magnitudes. There are only small changes in the S and P waves but 20–30 % or more changes in the D and F waves.

In order to explore the stability of the solution, we have pruned the data base at various levels. It is important to eliminate inconsistent data for two reasons: Not only do they increase χ^2 greatly, but they can also produce large changes in the error matrix even if the bad data do not affect the solution parameters. Our procedure is to eliminate all data points contributing a χ^2 greater than some minimum (six for π^+p, five for π^-p) to a given data set. The data are then renormalized and the parameters are re-searched to locate a new χ^2 minimum. We find that the removal of only 4% of the π^+p data points reduces χ_D^2 to 1 without altering the S and P waves more than 2% at 350 MeV. The majority of the data removed are $\sigma^+(\theta)$; only three σ_T^+ data are dropped. The π^-p data are generally of lower reliability, and a correspondingly larger number of data points must be removed (12% of the data points) to obtain a solution with 50% reliability. Again, in spite of the large amount of data removed, the phase shifts are virtually unaffected by the data pruning. The data removed[28] from our data base are listed in Tables IV and V.

The fit to the σ_T^+ data is largely determined by the Carter *et al.* measurements (T5 and T6); the

TABLE II. Compilation of πN energy-dependent solutions.

Solution	χ_D^2	K-matrix parametrization	Notes [a]
π^+p analyses			
A0	1.47	Resonance pole + background	Basic fit to full data base
A1	1.03	Resonance pole + background	Pruned solution, exclude $\chi_c^2 \geq 6$
A2	1.00	Inverse polynomial (form 2)	Pruned solution, exclude $\chi_c^2 \geq 6$
A3	1.04	Polynomial (form 3)	Pruned solution, exclude $\chi_c^2 \geq 6$
π^-p analyses			
B0	2.08	Resonance pole + background	Basic fit to full data base, $S_{31}(SL) + P_{33}$ splitting
B1	1.00	Resonance pole + background	Pruned solution, $S_{31}(SL) + P_{33}$ splitting (exclude $\chi_c^2 \geq 5$)
B2	0.98	Inverse polynomial (form 2)	Pruned solution, $S_{31}(SL) + P_{33}$ splitting, exclude $\chi_c^2 \geq 5$
B3	1.01	Polynomial (form 3)	Pruned solution, $S_{31}(SL) + P_{33}$ splitting, exclude $\chi_c^2 \geq 5$

[a] χ_c^2 denotes the critical value of χ_D^2 above which data were excluded in the pruned fits.

TABLE III. Quality of energy-dependent fits to the pion-nucleon data.

Solution[a]	No. of free parameters in the fit	χ^2	χ_D^2	σ_T^+	$\chi_D^{2\,b}$ $\sigma^+(\theta)$	$P^+(\theta)$	Ref$^+$(0)
π^+p analyses							
A0	14	1171.6	1.47	2.6	1.43	1.57	0.62
No. of data points				31	577	158	31
A1	14	758.6	1.03	0.92	1.07	0.99	0.56
No. of data points				28	554	149	31

	No. of free parameters in the fit	χ^2	χ_D^2	σ_T^-	σ_T^0	$\chi_D^{2\,b}$ $\sigma^-(\theta)$	$\sigma^0(\theta)$	$P^-(\theta)$	$P^0(\theta)$	Ref$^-$(0)
π^-p analyses										
B0	22	1536.2	2.08	2.41	1.85	2.37	1.98	1.82	0.43	0.43
No. of data points				33	11	372	101	190	1	31
B1	22	643.8	1.00	0.88	1.97	1.12	0.76	0.98	0.35	0.28
No. of data points				26	10	320	87	170	1	31

[a] For definitions of solutions, see Table II.
[b] χ_D^2 here represents the χ^2 per data point for a given data type.

TABLE IV. Data removed in pruning: solution A0. DXS=differential cross section; TXS=total cross section; POL =polarization.

E_L (MeV)	Data type	No. of data points	$\chi_D^{2\,a}$	λ	$\Delta\lambda$	θ	Reference
59.5	DXS	17	2.95	0.92	0.03	147, 155.4	D15
83.5	DXS	11	3.55	0.88	0.09	22.5	D23
94.5	DXS	3	3.01	0.99	0.07	90.5	D12
100.0	DXS	11	1.48	0.99	0.09	22.5	D27
113.0	DXS	10	1.76	0.93	0.09	16.7	D47
114.1	DXS	5	5.37	0.98	0.07	90.5, 112.4	D12
142.0	DXS	17	2.12	1.30	0.09	126.7	D40
142.9	DXS	14	1.91	1.01	0.007	35.4	D12
170.0	DXS	10	2.97	0.96	0.04	32.1, 135.3	D4
189.0	DXS	6	3.05	0.83	0.09	45.0	D35
194.3	DXS	15	0.91	1.00	0.007	73.4	D12
200.0	DXS	7	2.51	0.97	0.04	26.3	D43
236.3	DXS	14	1.28	1.00	0.007	138.3	D12
242.8	POL	17	3.66	0.93	1.00	117.4, 151.7, 161.7, 171.9	P9
247.0	POL	25	1.45	0.86	0.15	98.7	P8
247.5	DXS	13	2.38	1.05	1.00	90.1	D53
277.4	DXS	9	3.05	0.95	0.05	71.1, 153.9	D32
282.8	TXS	1	7.81				T6
290.2	DXS	12	2.59	0.98	0.05	167.9, 175	D32
300.2	POL	16	2.43	1.10	1.00	180	P9
306.0	POL	25	1.68	1.02	0.15	67, 115.7, 123.7	P8
310.0	DXS	23	2.23	1.04	0.06	108, 165	D55
317.0	TXS	1	34.90				T7
345.0	TXS	1	7.19				T5

[a] χ_D^2 here represents the χ^2 per data point for a given data type.

TABLE V. Data removed in pruning: solution B0. DXS=differential cross section; TXS=total cross sections; POL =polarization; CX=charge exchange.

E_L (MeV)	Data type	No. of data points	χ_D^2 [a]	λ	$\Delta\lambda$	θ	Reference
35.0	DXS	10	1.56	1.01	0.03	53.1, 157.7	D16
39.0	DXS	10	1.27	1.00	0.03	75.5	D18
59.5	DXS	18	5.04	0.90	0.03	47.2, 69.8, 101.1, 110.9, 120.3, 146.9	D15
76.7	TXS	1	12.3				T6
98.0	TXS	1	5.25				T8
98.0	DXS	13	2.52	1.02	0.02	82, 130.6	D20
114.4	TXS	1	7.34				T6
119.3	DXS	5	6.13	0.99	0.007	53.7, 136.2	D12
152.0	DXS	19	1.30	1.02	0.04	38, 90.5, 118	D39
164.7	TXS	1	13.7				T6
165.9	TXS	1	7.48				T4
170.0	DXS	8	1.78	1.11	0.15	38.3	D4
191.9	DXS	10	2.25	0.99	0.007	89.3, 138	D12
200.0	DXS-CX	6	5.19	0.99	0.10	60, 87.7, 147.1	D34
206.8	DXS	5	2.54	0.97	0.05	58.7	D8
217.0	DXS	6	1.42	1.03	0.05	65.7	D29
219.6	DXS	10	1.35	1.00	0.007	54.4, 79.1	D12
220.0	DXS	8	1.93	1.07	0.05	110, 149.3	D5
225.0	DXS	7	4.25	0.94	0.10	168.5	D34
229.0	POL	12	2.11	0.95	0.10	166, 176.3	P4
242.8	POL	10	1.44	0.97	1.00	156.9	P9
247.0	POL	25	2.03	1.19	0.15	83.6, 88.2, 90.6, 162	P8
263.7	DXS	10	4.39	1.00	0.007	55.1, 68.3, 80.6, 138.9	D12
270.0	DXS	6	3.25	1.08	0.10	87.7, 129.3	D43
288.0	DXS	10	6.37	0.95	0.05	69.4, 153.9, 167.9, 175	D32
291.5	DXS	10	2.23	1.00	0.007	69.3, 81.8, 145.5	D12
306.0	POL	25	2.71	0.75	0.15	99.6, 101.9, 103.5, 111.1	P8
310.0	DXS	28	6.72	0.98	0.03	54.4, 66.8, 78.5, 84.1, 89.6, 94.9, 109.8, 147, 151.6, 155.2, 158.9, 164.2, 166	D49
317.0	TXS	1	6.58				T7
318.0	POL	30	1.98	0.98	0.10	66.8, 92.6, 99.3, 111.8, 120.5	P4
333.5	DXS	6	3.94	0.92	0.04	108.1, 149.3	D8
334.0	DXS	10	8.38	0.82	0.05	71.4, 101.4, 154.6, 168.2, 175.5	D32
337.0	POL	30	1.65	0.82	0.10	128.1, 178.9	P4
337.0	DXS	7	3.99	1.07	0.10	60, 109.9, 129.1	D34
348.8	POL	14	1.81	0.90	1.00	109.3, 136.1	P9

[a] χ_D^2 here represents the χ^2 per data point for a given data type.

other values have little impact except to increase χ^2. The poor fit to these data in A0 is due solely to two Carter *et al.* data points and the datum of Davidson *et al.* (T7) at 317 MeV (the other Davidson *et al.* data were eliminated prior to the analysis). The bulk of the poorly fitted σ_T^- data lies on the high-energy side of the resonance peak. More than 20% of these data contributed a χ_D^2 greater than five and were eliminated in the pruning. The Bugg *et al.* σ_T^0 data (T4), on the other hand, are quite well fitted (see Tables I and III). All of the Davidson *et al.* $\sigma_T^\pm$ data were eventually eliminated in the pruning.

The precise low-energy π^+p differential cross-section data of Bertin *et al.* (D9) are well fitted in A0, whereas the data of Bussey *et al.* (D12) and

Gordeev *et al.* (D32) are not well represented in either A0 or B0. Our fit faithfully reconstructs the $\sigma^0(\theta)$ measurements of Comiso *et al.* (D14), Duclos *et al.* (D19), and Jenefsky *et al.* (D36) but is not in full agreement with the data of Bayer *et al.* (D7), Berardo *et al.* (D8), or Hauser *et al.* (D34).

The new measurements of $P^{\pm}(\theta)$ by Amsler *et al.* (P2 and P3), Alder *et al.* (P1), and Dubal *et al.* (P6) are also well fitted in our analysis, whereas the older data of Gorn *et al.* (P8 and P9) are found to be inconsistent with the other data and, in fact, have little impact on the values of the phase shifts.

In Fig. 2 we exhibit our fits to some of the total- and differential-cross-section and polarization data outlined in Table I. In view of the large amount of data used in the analysis it is not feasible to show a comparison between the calculated and experimental observables for all data points. Plotter outputs of data not exhibited are available on request.

The phase parameters used in the resonance fits A1 and B1 are given in Table VI. We have examined with care the variety in the structure of the partial waves and in the statistical quality of the fit when different numbers of free parameters are used to fit the data. This is required because, in general, the experimental data fluctuate around the true value of the observable. If more terms are included in the polynomial series than is optimally required, we effectively fit the noise in addition to the physical observable. In our usage, an optimum parametrization is obtained when the addition of an extra parameter in any partial wave leads only to a small improvement in the χ^2, whereas the deletion of any given parameter leads to a significant deterioration in the fit. We regard the parameters given in Table VI as yielding the most economical description of the πN scattering data in the first resonance region that has been made to date.

The root-mean-square errors on the parameters in Table VI are obtained by taking the square roots of the diagonal elements of the error matrix. This error matrix is modified to include the presence of normalization parameters. The relevant formulas are given by Arndt and Roper.[26] The errors are to be interpreted as the change ΔP_n in a given parameter which leads to a χ^2 increase of one when the given parameter is fixed at the value $P_n \pm \Delta P_n$, and all the other parameters are searched for a new minimum. A word of caution regarding the interpretation of these errors is required, however. They depend on the validity of the quadratic approximation for the analytic behavior of χ^2 at its minimum, on the specific parametrization, and on the completeness of the data base. The χ^2 space is generally pock marked by many local minima, making the range of validity of the quadratic approximation quite small, and thus an uncritical interpretation of the errors is unacceptable. When an accurate estimate of the error on a given parameter has been important (e.g., the error on the Δ pole position), we have made it a point to check and verify the quoted error by making the appropriate χ^2-parameter plot.

The phase shifts for solutions A1 and B1 are exhibited graphically in Figs. 3(a)–3(n). The errors on these phases, obtained from the full error matrix, are presented as error bands, giving the maximum variation in a particular phase which is consistent with a χ^2 change of one. The maximum errors on the S waves average about 1% and roughly 3% for the nonresonant P waves. Note that the error on our representation for the P_{33}, at most only 0.1%, does not show up on the scale of Fig. 3(h). In Fig. 3(b) we present the S_{31} phase determined by the best fit to the $\pi^+ p$ data, denoted S_{31}^+, and the S_{31} phase determined by the $\pi^- p$ data, denoted S_{31}^-. A similar notation is followed for the P_{33}.

We truncated the partial-wave expansion at F waves, though only S, P, and D waves are actually required to obtain a good fit to the full data base. G waves are typically 0.2° or less. Unfortunately, the higher partial waves modify the results slightly because of significant interference terms with the lower partial waves. Most strongly affected are P_{31} and P_{13}, which increase by a few standard deviations when G and H waves are included in the fit. Peripheral-wave errors are usually quite large, especially near the end of the energy range.

We retained only as many parameters in solutions A and B to describe the D and F waves as were required to optimize the solution; additional parameters may present a more complicated energy behavior but do nothing to improve the overall fit. The signs and magnitudes of the D and F waves are uniquely correlated to the signs and magnitudes of the S and P waves, as long as all the parameters are allowed to vary freely.

In Figs. 3(a)–3(n) we present our S-, P-, D-, and F-wave phase shifts from solutions A1 and B1 together with those obtained from the recent energy-dependent analyses of Rowe, Salomon, and Landau[29] (hereafter, RSL) (and other references as indicated). These authors report hadronic phases obtained by fitting the single-energy phases of previous analyses, supplemented by recent data. Breit-Wigner formulas incorporating a polynomial background were used in their parameterizations, no charge splitting was included, and no F waves were determined. To facilitate comparison, we have made the electromagnetic

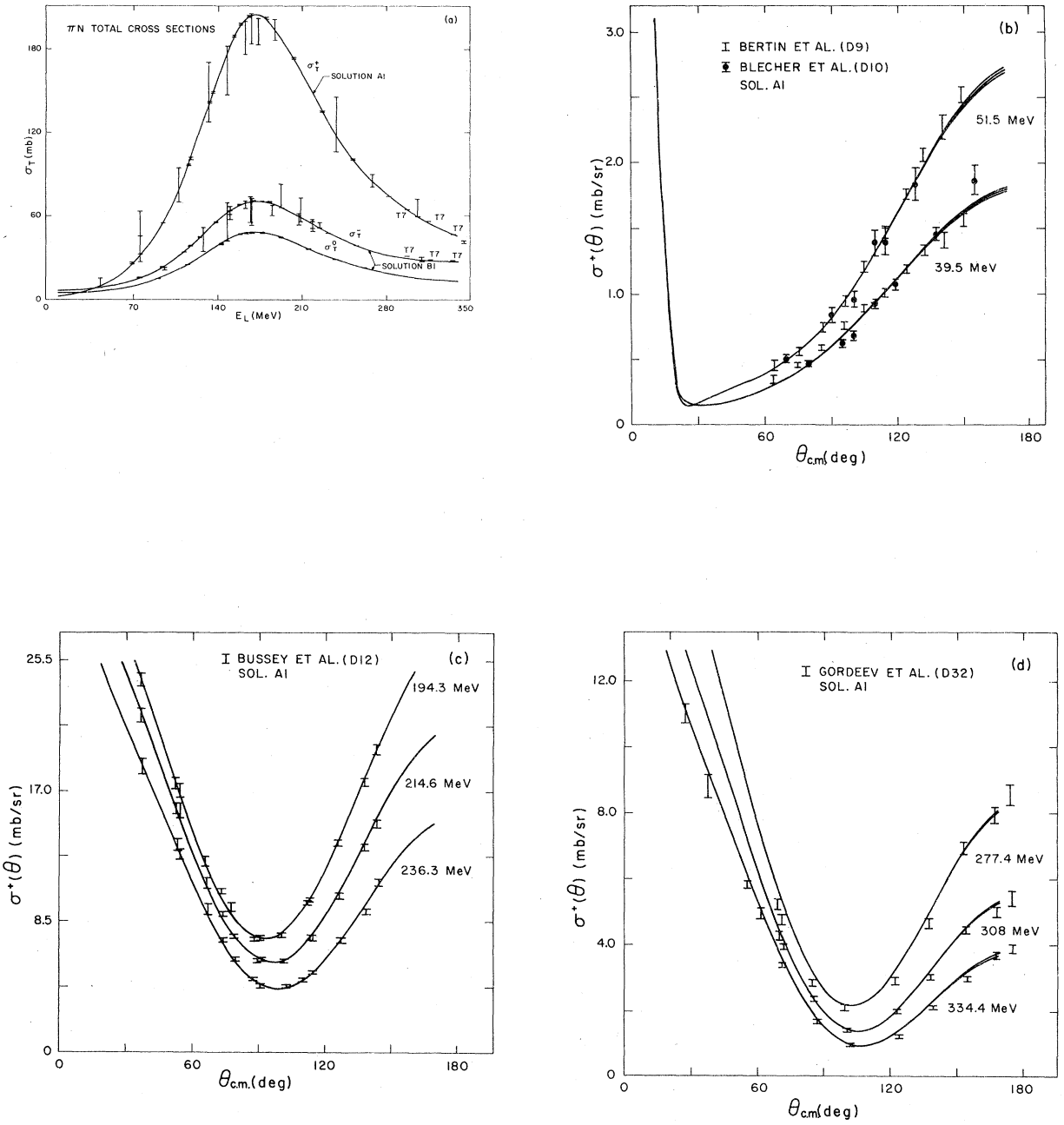

FIG. 2. Fits to the data. Each fit has three curves which indicate the values and error channels. (a) Total cross sections. (b) π^+p differential cross sections at 51.5 and 39.5 MeV. (c) π^+p differential cross sections at 194.3, 214.6, and 236.3 MeV. (d) π^+p differential cross sections at 277.4, 308, 334.4 MeV. (e) Differential cross sections for π^+p at 67.4 MeV and $\pi^-p \to \pi^-p$ at 88.5 MeV. (f) $\pi^-+p \to \pi^-+p$ differential cross sections at 119.3, 144.1, and 161.9 MeV. (g) $\pi^-+p \to \pi^-+p$ differential cross sections at 191.9, 219.6, 237.9, and 263.7 MeV. (h) $\pi^-+p \to \pi^-+p$ differential cross sections at 291.5 and 334 MeV. (i) $\pi^-+p \to \pi^0+n$ differential cross sections at 186.8, 212.3, 260.6, and 333.5 MeV. (j) $\pi^-+p \to \pi^0+n$ differential cross sections at 200, 206.8, 225, 247, 270, and 337 MeV. (k) $\pi^- + p \to \pi^0+n$ differential cross sections vs energy at 0°, 159.9°, and 180° (dashed curve). (l) π^+p polarization at 94.5 and 194.3 MeV (note the strong Coulomb interference at low angles and low energies). (m) π^+p polarization at 166 and 236.3 MeV. (n) π^+p polarization at 291.4 MeV. (o) π^+p polarization at 310 MeV. (p) π^-p polarization at 291.5 MeV. (q) π^-p polarization at 308 and 348.8 MeV and $\pi^-p \to \pi^0n$ polarization at 310 MeV [curve labeled $P^0(\theta)$]

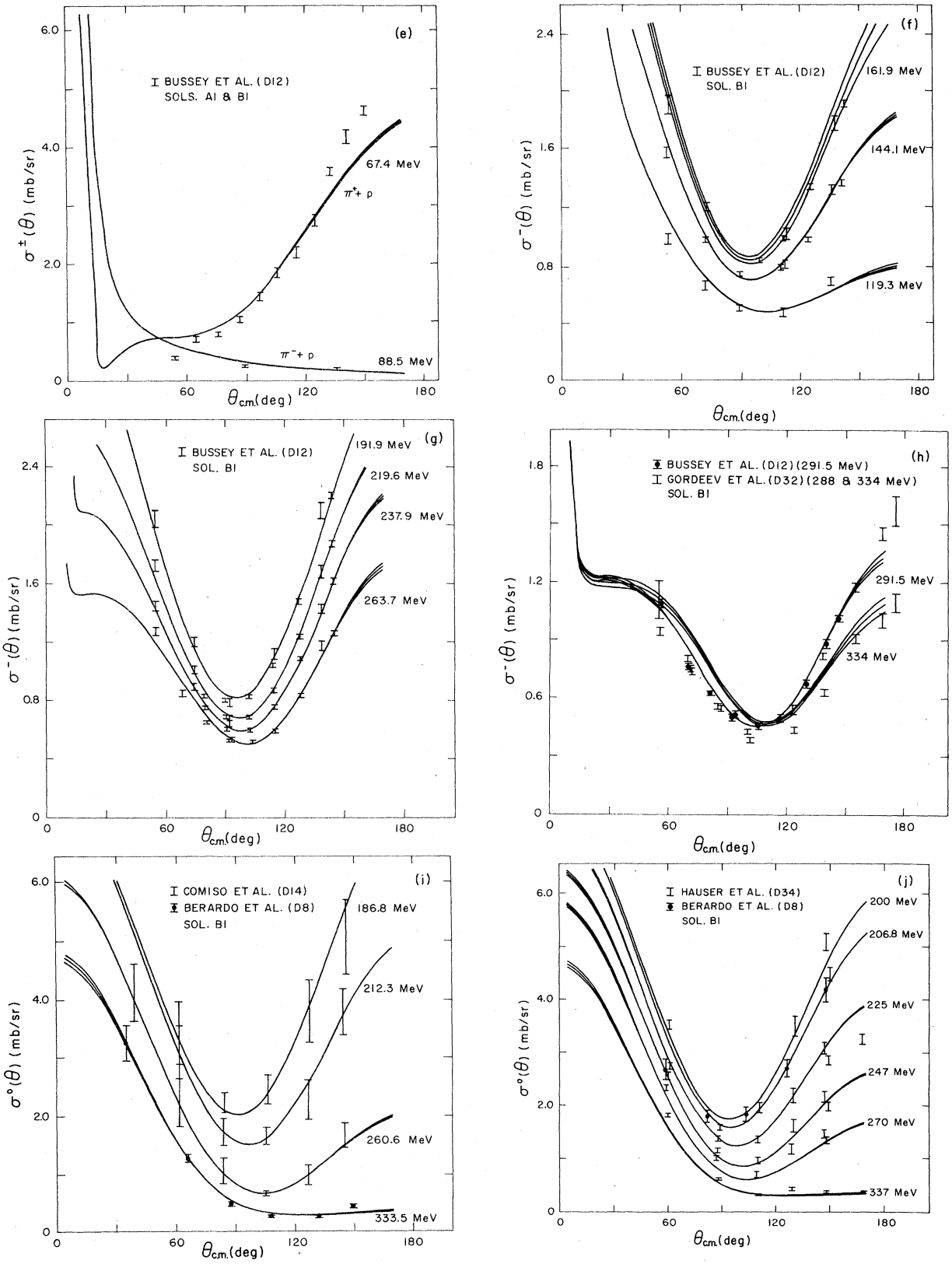

FIG. 2. (*Continued*).

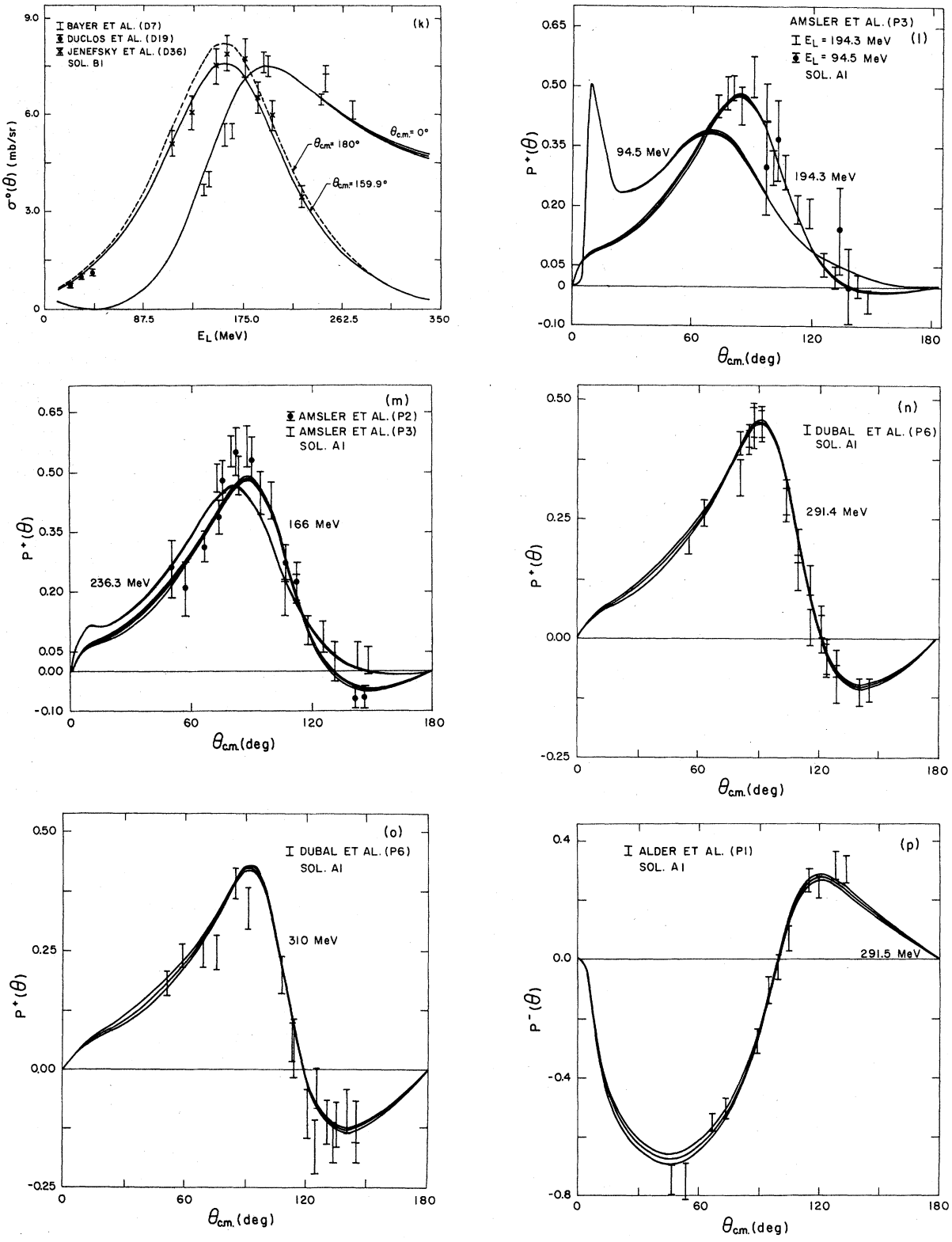

FIG. 2. (*Continued*).

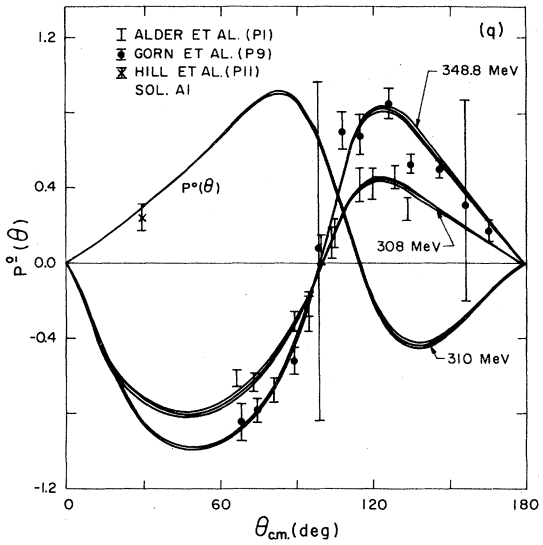

FIG. 2. (*Continued*).

corrections to our phase shifts proposed by Tromberg *et al.*[22] It is worth pointing out that these corrections are the same size or larger than the errors on our phases in most cases. The nuclear and hadronic phases differ roughly by a correction of order α.

Also shown in Fig. 3 are the results of the energy-independent partial-wave analyses of the SIN group (P1, P2, P3, and P6) covering the energy range 166–308 MeV and the most recent results from Saclay.[6] The SIN phases were obtained using the Carter, Bugg, and Carter data[2] (CBC) supplemented by the new SIN polarization data. Again, in order to facilitate comparison we removed the appropriate Coulomb corrections to obtain the corresponding nuclear phases. We note that the SIN results render the CBC phases obsolete.

It is well known that the peripheral waves may ponderably affect the values of the lower partial waves by virtue of interference terms in the amplitude. Various theories yield values for these waves which may be used as input into our programs. In particular, CBC use the theoretical predictions of Donnachie and Hamilton (DH)[30] as fixed input. These phases are shown in Figs. 3(d)–3(n). Note that the signs of these waves agree with the signs of the D and F waves given by solution A1. We also have access to the low-energy results of Alcock and Cottingham (AC).[31] These predictions have been incorporated into our analyses by fixing first the F waves and next both the D and F waves, at their theoretical values, and minimizing χ^2 with respect to the S- and P-wave parameters. We find that there is sufficient flex-

TABLE VI. πN phase parameters for solutions A1 and B1.

Phase shift	n	P_n	ΔP_n [a]	Form [b]	Phase shift	n	P_n	ΔP_n	Form [b]
π^+p analyses					π^-p analysis				
S_{31}	1	−4.1812	±0.0570	2	S_{31}	1	−3.9814	±0.0217	2
	2	13.4960	±0.5511			2	14.253		
	3	−21.2810	±1.3389			3	−22.842		
					P_{33}^-	1	0.2317	±0.0118	3
						2	−0.1642	±0.0395	3
P_{31}	1	−0.5339	±0.0178	3	S_{11}	1	0.4765	±0.0077	3
	2	0.6773	±0.0890			2	−1.6156	±0.1047	
P_{33}^+ [c]	1	0.1913	±0.0028	3		3	2.9856	±0.2840	
	2	−0.1331	±0.0097		P_{11}	1	−2.0847	±0.0346	3
D_{33}	1	0.1420	±0.0385	3		2	23.9440	±0.2806	
	2	−0.3288	±0.1278			3	−92.069	±1.3588	
D_{35}	1	−0.0729	±0.159	3		4	142.48	±2.8800	
F_{35}	1	−0.0105	±0.0130	3		6	1.8736	±0.0461	
F_{37}	1	0.0487	±0.0167	3	P_{13}	1	−0.4019	±0.0197	3
						2	1.6015	±0.1580	
m_{++} = 1210.7 ± 0.08 MeV						3	−2.7480	±0.3742	
Γ_{++} = 99.21 ± 0.23 MeV					D_{13}	1	0.1346	±0.0554	3
m_0 = 1210.3 ± 0.36 MeV						2	0.3851	±0.1833	
Γ_0 = 108.0 ± 0.52 MeV					D_{15}	1	0.2650	±0.0604	3
						2	−0.4077	±0.1931	
					F_{15}	1	0.0912	±0.0096	3
					F_{17}	1	0.0364	±0.0173	3

[a] ΔP_n is the change in P_n that increases χ^2 by one when all other parameters are searched.

[b] Refers to the type of phase-shift parametrization; see Eq. (11) in the text. No corrections of the form, Eqs. (22) and (23), are retained.

[c] For the P_{33} we utilize the resonance form given in Eqs. (32)–(35) with a form 3 background.

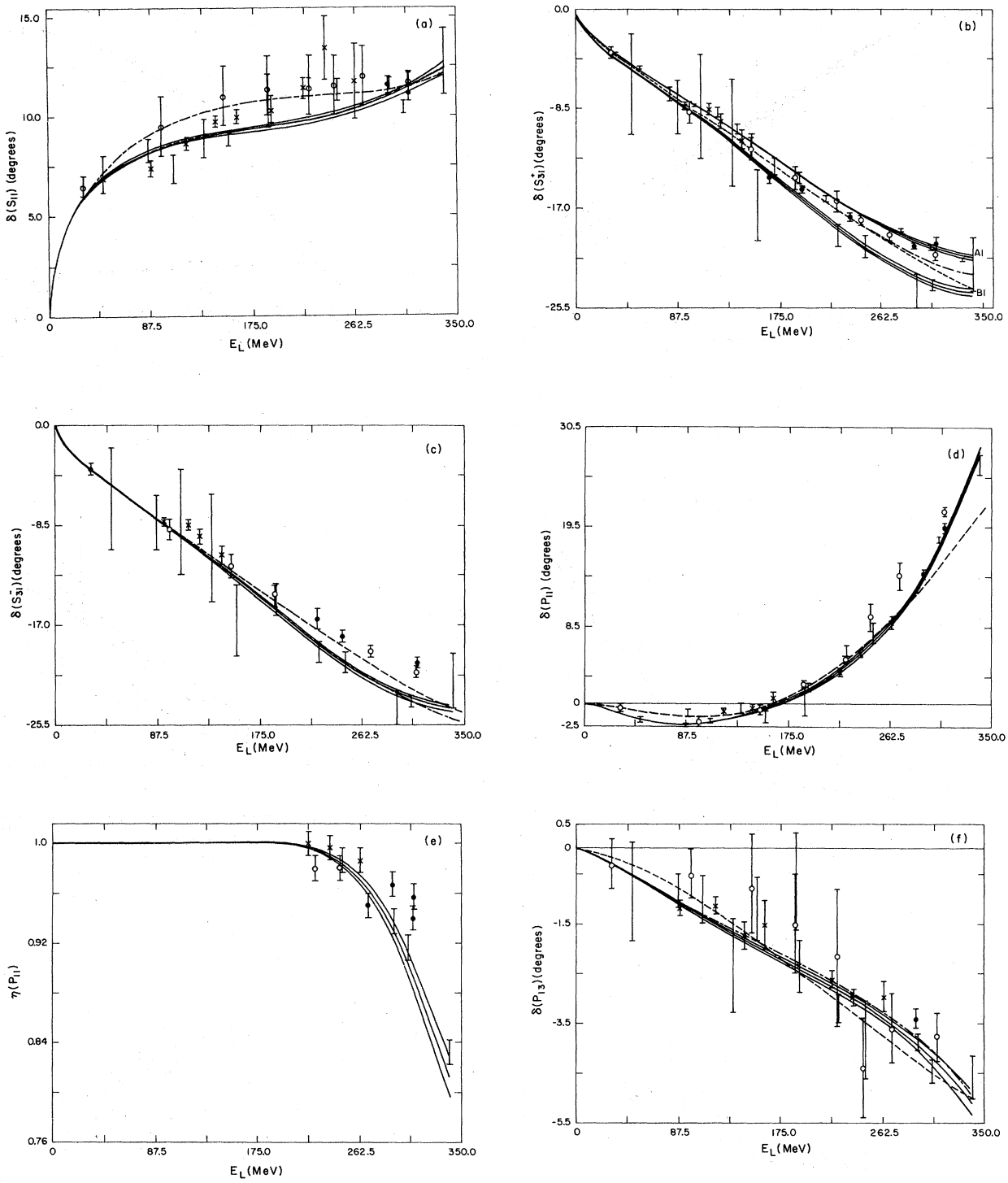

FIG. 3. Our solution and other recent solutions. Our "nuclear" phase shifts are represented by a solid line, our "hadronic" phase shifts by a dot-dash line, and RSL (Ref. 29) by a dashed line. Our energy-band phases are represented by $\mathbb{I}$, the SIN phases ($P1$, $P2$, $P3$, and $P6$ in Appendix A) by Φ, CBC phases (Ref. 2) by Φ and Ayed phases (Ref. 6) by Φ. (a) S_{11} phase shift. (b) S_{31}^{+} phase shift. (c) S_{31}^{-} phase shift. (d) P_{11} phase shift. (e) P_{11} absorption parameter. (f) P_{13} phase shift. (g) P_{31} phase shift. (h) P_{33} phase shift (note that the three solutions are indistinguishable). Pole position and Breit-Wigner position are indicated by dashed lines. (i) D_{13} phase shift. (j) D_{15} phase shift. (k) D_{33} phase shift. (l) D_{35} phase shift. (m) F_{15} and F_{17} phase shifts. (n) F_{35} and F_{37} phase shifts.

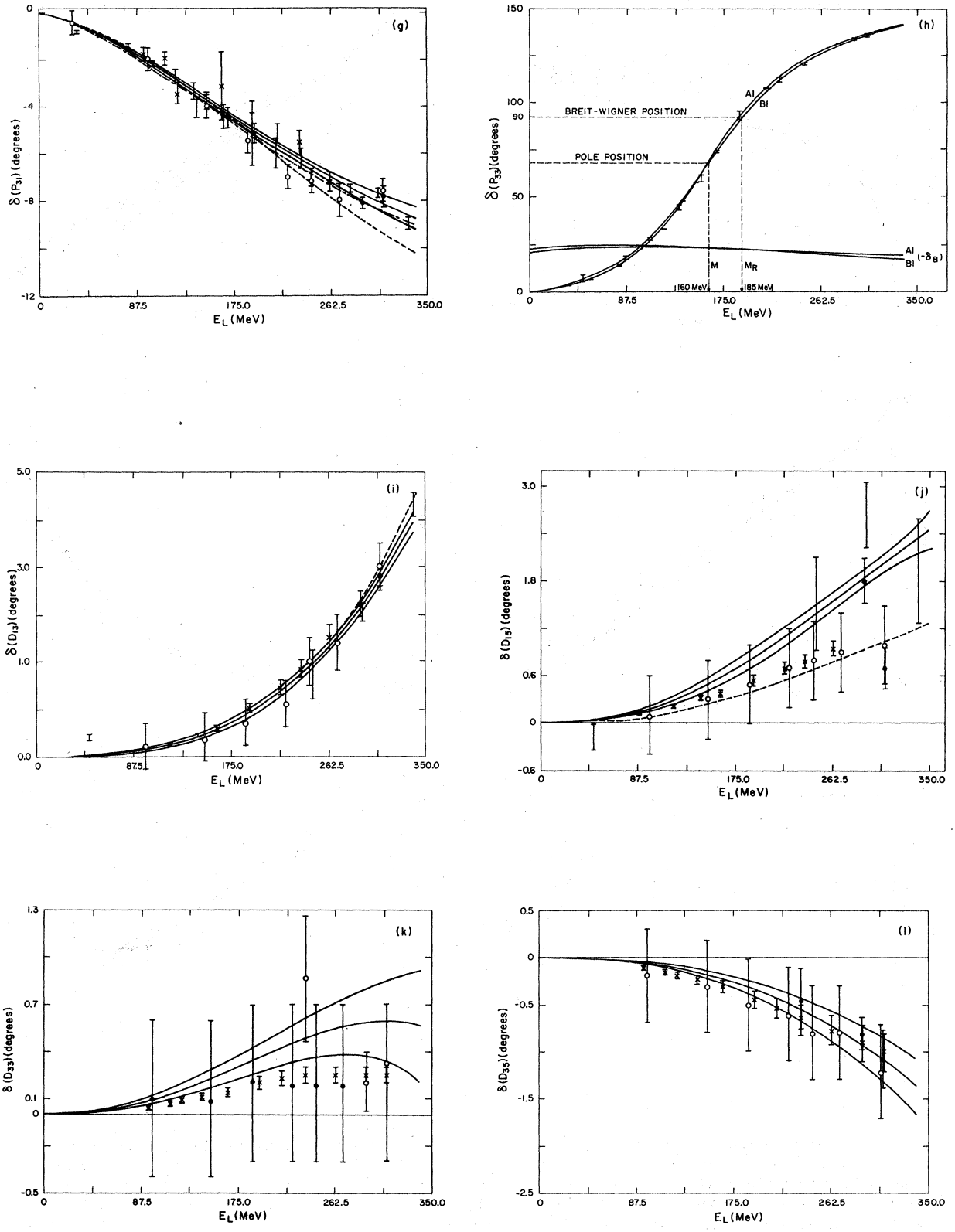

FIG. 3. (*Continued*).

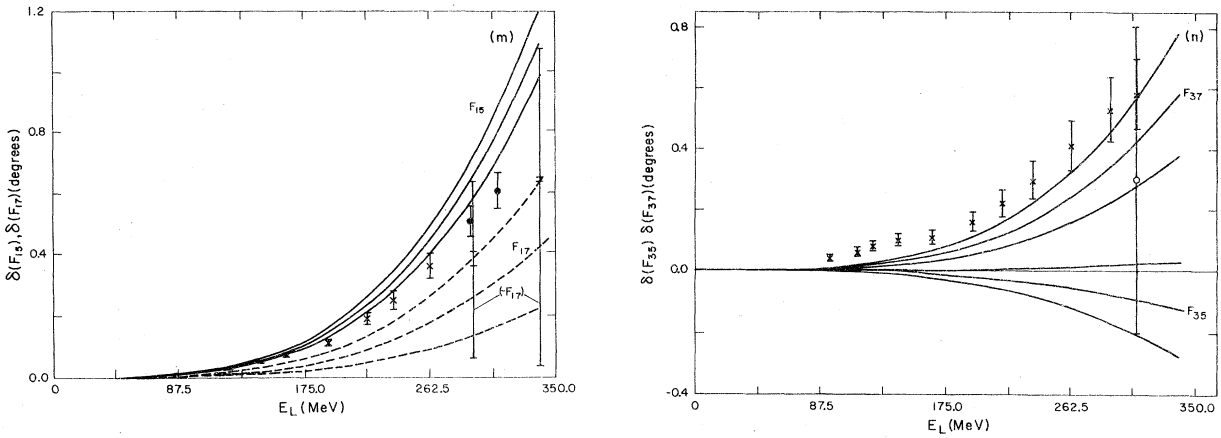

FIG. 3. (*Continued*).

ibility in the parameterization to permit the F waves of either theory to be incorporated into the fit without significantly altering the S or P waves. However, the attempt to incorporate both the D and F waves predicted by these theories leads to a degeneration in the quality of the fit. It is worth pointing out that F_{15} and F_{37} are both about one order of magnitude larger than F_{35} and F_{17} and that these latter phases are both consistent with zero.

In any energy-dependent partial-wave analysis there are always doubts concerning the theoretical bias due to an overly-restrictive parametrization. One way to check this is by comparing the energy-dependent solution with a single-energy analysis performed over the same energy range and the same data base. This allows for a check on the validity of the errors obtained from the error matrix.

To this end energy-dependent analyses were performed on the πN data over small energy bands centered at the energies given in Tables VII and VIII. These energy bands were selected to optimize the variety and quality of the data in as small an energy range as possible. At each energy, the initial phases, as well as their local energy dependence, were acquired from solutions A1 or B1. Then the P_1 parameters were varied to readjust the relevant phase up or down as required to minimize χ^2. It was usually sufficient to vary only the S- and P-wave P_1 parameters to obtain a good fit, but in some cases D and F waves as well had to be included.

The results are plotted in Figs. 3(a)–3(n). The agreement with the energy-dependent solutions is seen to be very good. No systematic differences occur.

TABLE VII. Results of π^+p energy-band analyses.

ΔE_L (MeV)	No. of data points	χ^2(A1) [a]	χ^2	$\delta(S_{31}^+)$	$\delta(P_{31})$	$\delta(P_{33}^+)$
30–40	41	39	16	−3.79 ± 0.09	−0.80 ± 0.06	3.33 ± 0.06
50–60	37	66	58	−4.99 ± 0.13	−0.98 ± 0.05	6.63 ± 0.09
78–84	28	58	54	−7.26 ± 0.61	−1.50 ± 0.16	13.94 ± 0.38
94–110	50	65	64	−8.27 ± 0.13	−2.20 ± 0.10	22.82 ± 0.05
118–125	42	48	32	−8.89 ± 0.40	−2.75 ± 0.32	32.92 ± 0.09
135–143	39	86	65	−10.31 ± 0.44	−3.37 ± 0.34	47.71 ± 0.10
140–162	54	96	73	−11.25 ± 0.53	−3.77 ± 0.36	57.39 ± 0.16
165–176	63	83	80	−13.50 ± 0.72	−4.50 ± 0.44	73.92 ± 0.40
184–200	51	65	64	−14.48 ± 0.50	−4.78 ± 0.48	92.53 ± 0.43
200–230	50	48	48	−16.27 ± 0.29	−5.18 ± 0.41	107.16 ± 0.16
235–255	99	181	179	−17.88 ± 0.19	−7.13 ± 0.31	120.62 ± 0.15
260–301	90	159	141	−18.95 ± 0.14	−7.50 ± 0.17	130.67 ± 0.08
300–310	105	165	159	−20.40 ± 0.26	−7.71 ± 0.18	135.56 ± 0.43
315–350	40	86	68	−21.41 ± 0.17	−8.98 ± 0.26	139.80 ± 0.10

[a] χ^2(A1) denotes the χ^2 for solution A1 in the indicated energy band.

TABLE VIII. Results of $\pi^- p$ energy-band analyses.

E_L (MeV)	No. of data points	χ^2(B1)	χ^2	$\delta(S_{11})$	$\delta(S_{31})$	$\delta(P_{13})$	$\delta(P_{33})$	$\delta(P_{11})$
35–60	51	138	55	7.07	−6.28	−0.86	7.05	−1.73
				±0.94	±4.37	±0.99	±1.75	±0.28
76–98	20	51	22	8.26	−8.30	−0.85	17.52	−2.40
				±0.58	±2.33	±0.34	±0.64	±0.24
98–118	25	54	21	7.34	−8.25	−1.02	27.21	−1.90
				±0.72	±4.50	±0.49	±0.77	±0.29
127–141	31	23	20	8.85	−10.49	−2.35	44.01	−0.53
				±0.98	±4.58	±0.94	±1.24	±0.58
150–160	50	78	56	8.81	−16.65	−1.21	59.32	−1.45
				±0.34	±3.03	±0.65	±0.65	±0.63
184–194	31	38	31	10.73	−14.91	−0.65	92.90	0.20
				±1.36	±1.34	±0.99	±2.40	±1.56
220–230	69	105	89	10.80	−19.33	−3.22	111.47	5.73
				±1.04	±0.87	±0.28	±1.34	±0.72
240–256	54	96	76	11.28	−20.20	−3.82	120.08	7.84
				±0.56	±0.88	±0.78	±0.78	±1.11
285–300	57	127	56	11.57	−24.06	−3.89	132.74	13.93
				±0.29	±1.46	±0.18	±0.67	±0.46
300–310	109	296	160	10.36	−23.56	−4.47	134.52	18.07
				±0.33	±0.46	±0.24	±0.68	±0.33
330–350	75	218	104	12.67	−21.80	−4.60	142.11	26.29
				±1.67	±2.34	±0.43	±1.36	±1.13

V. RESONANCE PARAMETRIZATION

In the absence of a widely accepted unstable particle field theory, phenomenological resonance formulas are used to describe the phase shift of a resonant state, taking into account the analytic properties expected from S-matrix theory. Based on analogy with the Breit-Wigner formula, the resonance mass m_R is typically defined as the energy at which the phase shift passes through 90°, i.e.,

$$\delta_R(W=m_R)=\pi/2\,, \tag{28}$$

where δ_R denotes the resonant phase shift. The resonance width Γ_R is then defined by the corresponding energy derivative:

$$[d\delta_R(W)/dW]_{W=m_R}=\frac{2}{\Gamma_R}\,. \tag{29}$$

It is conventional to extract the resonance parameters by fitting Breit-Wigner formulas to phase shifts or to total or elastic partial-wave cross-section data. An alternative method is to find the energy at which the "speed" of the amplitude in an Argand diagram is maximum. In any case, these are clearly model-dependent definitions, and it is well known that the resonance mass and width found by applying Eqs. (28) and (29) are very sensitive to the exact phase-shift parametrization when Γ_R/m_R is large, and substantial background is present. This feature has recently been emphasized by Cheng and Lichtenberg,[32] who have shown by comparing equally good fits to the data that different parametrization of the Δ resonance occurring in the P_{33} state in πN scattering yield a spread in the resonance mass exceeding 10 MeV and a spread in the width of more than 20 MeV.

It is significant that the position of the Δ resonance pole in the complex energy plane, however, is relatively insensitive to the parametrization. This is especially notable in that the pole position and its residue are the fundamental quantities occurring in S-matrix theory. Usually the position of the resonance pole is determined by a three-step process. First a single-energy analysis is made of the scattering data. Next the single-energy resonant phase is fitted with one of many continuous-energy relativistic Breit-Wigner formulas. Finally, an analytic continuation into the unphysical sheet is performed in order to locate the pole. This three-step procedure may be reduced to one step by exploiting a resonance formula proposed by Lichtenberg[8] and by conducting an energy-dependent partial-wave analyses of the data.

In his parametrization of an elastic resonance with background, the mass and width parameters appearing in the scattering amplitude locate the pole position directly so that analytic continuation is not necessary. In an energy-dependent analysis another advantage is that reliable errors based on the error matrix can be easily assigned to the pole

parameters.

In what follows we present a brief outline of the Lichtenberg resonance formula; for more details we refer the reader to the references. It is assumed that both the resonant and background parts of the S matrix describing the resonance are unitary and enter as the product

$$S = S_R S_B , \tag{30}$$

where S_R and S_B denote the resonance (R) and background (B) S matrices, respectively. For an elastic resonance the K-matrix element is then written

$$K = \frac{K_R + K_B}{1 - K_R K_B} , \tag{31}$$

where K_R and K_B are the resonance and background K matrices defined in the usual manner in terms of T_R and T_B.

In the parametrization proposed by Lichtenberg, the resonance K matrix is written

$$K_R = \frac{\Gamma/2}{m - W} , \tag{32}$$

where W is the barycentric energy of the pion and nucleon in MeV and the complex pole position of the resonance is

$$m^* = m - i(\Gamma/2) . \tag{33}$$

The threshold behavior is assumed to arise solely from the background contribution

$$K_B = K_R(\rho_l^* - 1) + \rho_l^* \overline{K}_B , \tag{34}$$

where ρ_l^* is the normalized phase-space factor

$$\rho_l^* = \rho_l(W)/\rho_l(m) , \tag{35}$$

and $\overline{K}_B$ is a phenomenological energy-dependent background term. Note that in this formulation the T matrix has a pole at $W = m^*$, independent of the form of $\overline{K}_B$. We have chosen to parametrize $\overline{K}_B$ as a polynomial or inverse polynomial, as in Eq. (11).

For incident pion laboratory kinetic energies less than 350 MeV, only a single resonance occurs in πN scattering, the $\Delta(1232)$ or Fermi resonance, occurring in the P_{33} state. We denote the pole positions of the relevant charge states of this resonance by

$$\begin{aligned} m_{++}^* &= m_{++} - i(\Gamma_{++}/2) , \\ m_0^* &= m_0 - i(\Gamma_0/2) , \end{aligned} \tag{36}$$

for the Δ^{++} and Δ^0, respectively.

We find that the best fit to the scattering data is obtained for a P_{33} phase described by two background parameters (see Table VI). Solutions A1 and B1 possess T-matrix poles at

$$\begin{aligned} m_{++} &= 1210.70 \pm 0.16 \text{ MeV} , \\ \Gamma_{++} &= 99.21 \pm 0.23 \text{ MeV} , \end{aligned} \tag{37}$$

for the Δ^{++}, and

$$\begin{aligned} m_0 &= 1210.3 \pm 0.36 \text{ MeV} , \\ \Gamma_0 &= 108.0 \pm 0.52 \text{ MeV} , \end{aligned} \tag{38}$$

for the Δ^0.

The masses and widths of the Δ resonances determined by our analysis possess errors about $\frac{1}{3}$ as large as previous determinations,[33-36] represented in Figs. 4(a) and 4(b). These errors were carefully checked from a detailed study of the χ^2 contours and are defined as usual by $\chi^2 = \chi_{\min}^2 + 1$ for a one-standard-deviation change in any parameter. The small errors on the pole positions, as compared to other studies, may be attributed to our large data base and the relatively small number of free parameters. These other determinations of the Δ pole position do not result from a direct analysis of the scattering data but by fits to the P_{33} phase shifts of Carter, Bugg, and Cart-

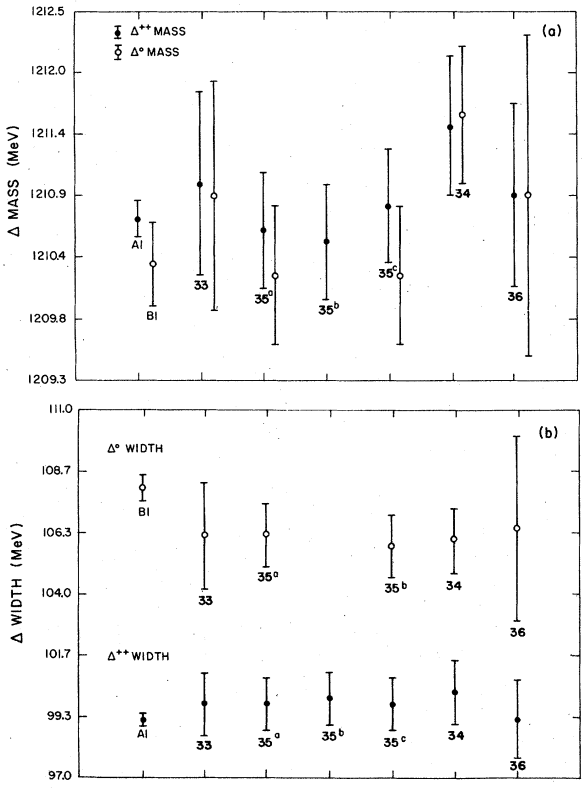

FIG. 4. Comparison of our P_{33} resonance parameters with previous determinations. The numbers near the data points are reference numbers. (a) Δ mass. (b) Δ width.

er.[2] Neither the mass nor the width exhibits any significant dependence on the inclusion of Coulomb threshold effects, or form dependence of the phase-space factor or background phase. For these reasons we advance Eqs. (37) and (38) as the most precise determination of the Δ pole positions made to date, and in harmony with other authors, it is our contention that the quantity of fundamental theoretical interest is the resonant pole position, not the resonance parameters obtained from Eqs. (28) and (29).

Using our parametrization for the P_{33} phase shift it is a simple matter to find the resonance parameters defined in Eqs. (28) and (29) corresponding to our values for the T-matrix poles:

$$m_R^{++} = 1230.6 \pm 0.2 \text{ MeV}, \qquad \Gamma_R^{++} = 113.2 \pm 0.3 \text{ MeV}, \tag{39}$$

and

$$m_R^{0} = 1232.5 \pm 0.3 \text{ MeV}, \qquad \Gamma_R^{0} = 121.3 \pm 0.4 \text{ MeV}. \tag{40}$$

These results may be used to emphasize the need for care in uncritically accepting the reported values for the mass and width of a resonance as the "real" mass and width. The 20-MeV difference between m_R and Re(m^*) shows there is clearly a danger inherent in testing, for example, any broken-symmetry mass relation by uncritically adopting the reported values for the Δ mass, as they usually refer to the parameters of a modified Breit-Wigner expression rather than the pole position.

The previous results may be used to calculate the Δ^0-Δ^{++} mass difference. From Eqs. (37) and (38),

$$m_0 - m_{++} = -0.40 \pm 0.39 \text{ MeV}, \qquad \Gamma_0 - \Gamma_{++} = 8.79 \pm 0.57 \text{ MeV}. \tag{41}$$

We expect $\Gamma_0 > \Gamma_{++}$ due to Coulomb-barrier repulsion between the charged pion and the proton. Though $m_{++} > m_0$ is qualitatively consistent with simple self-energy calculations, it contradicts the general rule that the baryon with the lower charge is always the heavier one (witness the $\frac{1}{2}^+$ octet, for example). Theoretical predictions of the mass difference based on quark-model assumptions do not favor the results obtained here. In Table IX we present a compilation of theoretical predictions for the mass and width differences.

Calculations of the decay rates for particular charge states of the Δ resonance are clearly in short supply. Several attempts have been made to calculate $\Delta \to \pi + N$ in the context of the nonrelativistic quark model[46-48] and the MIT bag model.[50] Both methods give $\Gamma(\Delta \to \pi + N) = 70$–$80$ MeV. Due to inconsistencies in the data, a critical test of these theories is not yet possible.

Though the mass and width differences we obtain are not sensitive to the parametrization of the amplitude, they are sensitive to the way charge splitting is incorporated in the nonresonant partial waves. In a previous publication we allowed for charge splitting in all partial waves and found[49]

$$m_0 - m_{++} = 0.9 \pm 0.54 \text{ MeV}, \qquad \Gamma_0 - \Gamma_{++} = 5.4 \pm 0.49 \text{ MeV}. \tag{42}$$

Though this fit violates I-spin conservation in all partial waves, it does lead to an appreciably better fit to the total-cross-section data ($\chi_D^2 = 1.5$).

One built-in limitation of our method of determining the Δ^{++}-Δ^0 mass difference is that with such a large data base we include data far from the singularity as well as data near the singularity. In the least-squares fit this faraway information may distort the resonance shape causing a shift in the pole position. To get some estimate of the size of this shift it is useful to fit the total-

TABLE IX. Compilation of theoretical values for the Δ^{++}-Δ^0 mass and width differences.

$M_0 - M_{++}$ (MeV)	Assumptions	Reference
2.4	Tadpole and baryon-octet self-energy diagrams	37
−3.38	Born term	38
−3.67 ± 0.73	Broken-SU(3) prediction	39
0.96	Quark model: harmonic-oscillator potential	40
0.3	Quark model: perturbed harmonic oscillator	41
0.61	MIT bag model	42
0.8	Charmed-quark model	43
−1.0	Dispersion relations	44
$\Gamma_0 - \Gamma_{++}$ (MeV)	Assumptions	Reference
5.2	Dispersion relations	44
3.5	Penetration-factor model	45

cross-section data alone (keeping all nonresonant phases fixed at their best values). The results, including the χ^2/datum, are

$$m^*_{++} = (1210.6 \pm 0.23) - \tfrac{1}{2}i(100.03 \pm 0.40), \quad \chi_D{}^2 = 0.84$$
$$m^*_0 = (1209.0 \pm 0.28) - \tfrac{1}{2}i(104.97 \pm 0.55), \quad \chi_D{}^2 = 1.5. \tag{43}$$

Fitting the Carter σ_T^- data alone gave $m_0 = 1209.4$, and fitting all the non-Carter data alone gave $m_0 = 1211$ MeV $\pm$ 0.48. The difference between Eqs. (37) and (43) emphasizes the role of the angular data in shifting the pole position.

As an independent check on Eqs. (37) and (38), we have analytically continued the P_{33} partial wave described by a form 2 polynomial in order to locate the poles:

$$m^*_{++} = (1210.81) - \tfrac{1}{2}i(99.17) \text{ MeV}, \qquad m^*_0 = (1210.95) - \tfrac{1}{2}i(108.29) \text{ MeV}. \tag{44}$$

The pole is obtained as a zero in the determinant of the matrix $1 - i\rho^{1/2}\bar{K}\rho^{1/2}$ on the unphysical sheet. These values are consistent, within errors, with the results presented in Eqs. (37) and (38). However, it is difficult using the procedure of analytic continuation to assign meaningful errors, a clear advantage in favor of the Lichtenberg formula.

Finally, we have performed the Coulomb corrections of Tromberg *et al.*[22] to the P_{33} phase shift and refitted the phase in order to determine the purely hadronic masses and widths of the Δ resonances. The results

$$m^*_{++} = (1209.0 \pm 0.17) - \tfrac{1}{2}i(99.32 \pm 0.31) \text{ MeV}, \qquad m^*_0 = (1211.0 \pm 0.40) - \tfrac{1}{2}i(106.9 \pm 0.74) \text{ MeV}, \tag{45}$$

show that some unaccounted for correction still remains to be analyzed and points up the uncertainties associated with such calculations. The errors on the values given in Eq. (45) were obtained by folding in quadrature the errors quoted in Eqs. (37) and (38) and the errors from the determination of the phase-shift parameters for the hadronic phases.

Celmaster[41] has predicted the existence of a $J^P = \frac{1}{2}^-$ elastic resonance in the S_{11} partial wave at

$$m(S_{11}) = 1335 \pm 60 \text{ MeV} = 330 \text{ MeV for } E_L, \qquad \Gamma(S_{11}) \leq 50 \text{ MeV}. \tag{46}$$

We have parametrized the S_{11} partial wave using the Lichtenberg form in order to search for evidence of such a resonance, with no success. Such a resonance, if it exists, must be too narrow to show up in the present data.

In S-matrix theory a resonance pole is defined by four fundamental parameters: two to describe its position in the complex energy plane and two to describe the complex residue of that pole. In the vicinity of the pole, the T matrix may be written as

$$T(W) = \frac{R}{W - m^*}, \tag{47}$$

where

$$R = -\tfrac{1}{2}ge^{i\phi} \tag{48}$$

is the residue. The residue is related to the background phase in a manner that depends on the way the resonance phase is parametrized. For a resonance represented by the Lichtenberg form, Eqs. (32)–(35), we have

$$g = \Gamma|S_B(m)|, \tag{49}$$

$$\phi = \arg[S_B(m)], \tag{50}$$

where S_B is the background S matrix. We observe that the imaginary part of the residue arises from the existence of the background amplitude. Our work permits us to determine the residues for both the Δ^0 and Δ^{++} poles. For fits A1 and B1,

$$g_{++} = 101.12 \pm 0.30 \text{ MeV}, \qquad \phi_{++} = -46.67 \pm 0.50^\circ, \tag{51}$$

$$g_0 = 111.60 \pm 0.30 \text{ MeV}, \qquad \phi_0 = -48.83 \pm 0.50^\circ. \tag{52}$$

A compilation of phenomenological values for the residue of the Δ resonances pole is given in Table X. It is clear from this table that the residue, like the pole position, is essentially a model-independent quantity. This does not amount to a model-independent determination of the background because in another parametrization of the resonance the residue would be related to the background in a different way.

In general we may write

$$R = -\frac{1}{2}\left(\frac{g_{\Delta N\pi}{}^2}{4\pi}\right)q^3\Gamma_R(m^*), \tag{53}$$

where $\Gamma_R(W)$ is a "reduced" energy-dependent width from which the $\Delta N\pi$ coupling constant $g_{\Delta N\pi}$ and the phase-space factor q^3 have been removed. In order to evaluate Eq. (53) and determine a value for the $\Delta N\pi$ coupling constant we must assume some model for the $\Delta \to \pi N$ transition. The most general gradient coupling of the Δ to the pion field gives[52]

$$\Gamma_R(W) = m\frac{E + m_N}{3W^2}, \tag{54}$$

where E is the barycentric energy of the nucleon. Using these results we obtain

TABLE X. Phenomenological determinations of the residue of the Δ pole.

g (MeV)	ϕ (MeV)	Re(R)	Im(R)	State	Reference
101.12 ± 0.30	−46.67 ± 0.50	−34.70 ± 0.40	36.8 ± 0.40	Δ^{++}	A1
111.60 ± 0.30	−48.84 ± 0.50	−36.70 ± 0.40	42.0 ± 0.40	Δ^{0}	B1
104.2 to 104.9	−47.2 to −45.4	−35.4	38.2 to 38.7	Δ^{++}	35 [a]
110.1 to 111.0	−48.7 to −48.9	−36.2 to −36.6	41.5 to 41.7	Δ^{0}	35
106	−48	−35.5	39.4	Δ [b]	
104.4 to 107.2	−46.2 to −45.6	−36.1 to −37.5	37.7 to 38.3	Δ	51 [c]
104.7	−47.3	−35.5	38.5	Δ	36

[a] Three different parametrizations were used to give the ranges shown.
[b] Δ means no distinction was made between different charge states.
[c] Five different parametrizations were made that give the ranges shown.

$$g_{\Delta^{++}p\pi^{+}}{}^{2}/4\pi = (0.41 - i0.08)\mu^{-2}\,,$$
$$g_{\Delta^{0}N\pi}{}^{2}/4\pi = (0.41 - i0.09)\mu^{-2}\,, \tag{55}$$

which may be compared to the value obtained by Olsson,[52]

$$g_{\Delta N\pi}{}^{2}/4\pi = (0.28 \pm 0.015)\mu^{-2}\,. \tag{56}$$

Henyey and Kane[51] have argued that the Δ residue can be simply understood as a background effect due to nucleon exchange and the opening of inelastic channels at 1600 MeV.

VI. PREDICTIONS

One distinct advantage of an energy-dependent representation of the scattering data as opposed to an energy-independent analysis is that it allows for reliable predictions of observables not experimentally measured within the energy range of the representation, even when the data set is incomplete. Outside this energy range, on the other hand, the continuous-phase representation will generally fail to extrapolate properly.

It is well known[53] that the nonrelativistic πN scattering amplitudes may be directly reconstructed from the experimental data if the differential cross section, final-proton polarization, and the two spin-rotation parameters R and A are precisely measured at the same energy and angle. The situation is even more complicated at relativistic energies; it is necessary to measure at least twice as many observables to determine the pion-nucleon isospin amplitudes.[54] The absence of such complete data sets leads to multiple solutions, a problem often referred to as "phase-shift ambiguities." Energy-independent analyses are especially susceptible to such ambiguities due to their lack of energy continuity and the nonlinearity of the relation between the phase shifts and observables. Unitary energy-dependent representations remove most of these ambiguities, especially when supplemented with theoretical input, for example, values for $\mathrm{Re}f^{\pm}(0)$, which remove the sign-change ambiguity.[55]

To date no measurements of the spin-rotation parameters have been made in the first resonance region although such data could resolve continuous-phase ambiguities[53] in the πN amplitudes and lead to an important improvement in the quality and reliability of partial-wave analyses. Such ambiguities, which leave the fit to the data unchanged, have even been shown[56] to be present for any finite number of partial waves when only $\sigma(\theta)$ and $P(\theta)$ data exist. The measurement of spin-rotation parameters at energies in the first and second resonance regions will soon be made at LASL.[13] Such measurements are quite difficult because they require a double scattering experiment with a polarized target.

Many different definitions of spin-rotation parameters are in use; so it appears judicious to report values for the quantities

$$B(\theta) = 2\,\mathrm{Re}[f^{*}(\theta)g(\theta)]/\sigma(\theta)\,, \tag{57}$$
$$S(\theta) = [|f(\theta)|^{2} - |g(\theta)|^{2}]/\sigma(\theta)\,, \tag{58}$$

where $f(\theta)$ and $g(\theta)$ are the spin-nonflip and spin-flip amplitudes, respectively. All other spin-rotation parameters in common use may be constructed by taking linear combinations of B and S. In particular, the A and R parameters are defined by the equations

$$A(\theta) = S(\theta)\sin\theta + B(\theta)\cos\theta\,, \tag{59}$$
$$R(\theta) = -S(\theta)\cos\theta + B(\theta)\sin\theta\,. \tag{60}$$

In Figs. 5(a)–5(o) we present predictions of $\sigma(\theta)$, $P(\theta)$, $B(\theta)$, and $S(\theta)$ for each of the three charge states at several energies of experimental interest. Other predictions of observables are available on request.

VII. CONCLUSIONS

Based on our study it is clear that the $\pi^{+}p$ scattering data in the first resonance region are of sufficient accuracy and consistency to permit a

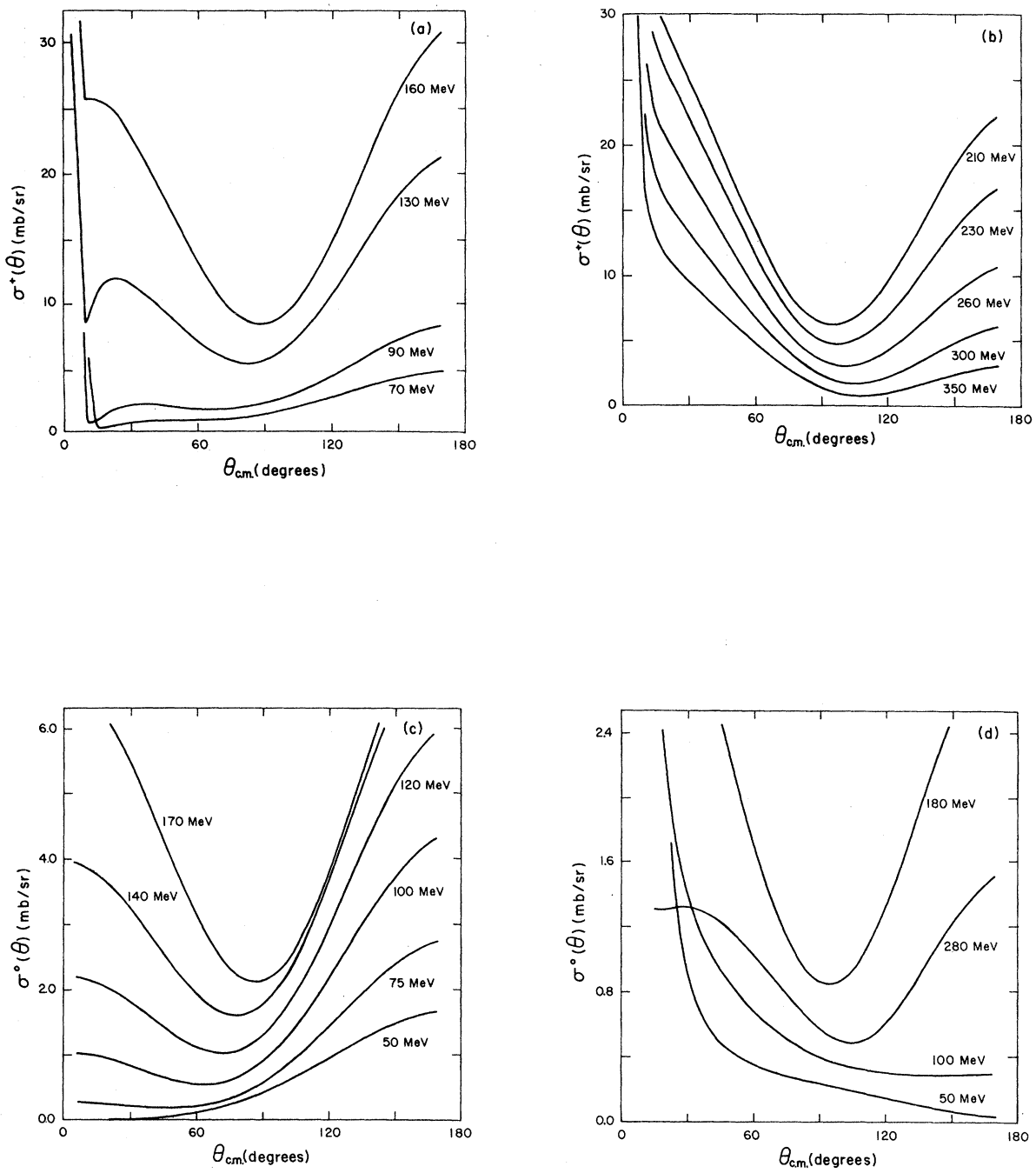

FIG. 5. Our solutions A1 and B1 predictions for pion-nucleon observables from 0 to 350 MeV. (a) π^+p differential cross sections at 70, 90, 130, and 160 MeV. (b) π^+p differential cross sections at 210, 230, 260, 300, and 350 MeV. (c) π^-p differential cross sections at 50, 100, 180, and 280 MeV. (d) $\pi^-+p\rightarrow\pi^0+n$ differential cross sections at 50, 75, 100, 120, and 170 MeV. (e) $\pi^-+p\rightarrow\pi^0+n$ differential cross sections at 180, 230, 250, 280, and 320 MeV. (f) π^+p polarization at 100, 150, and 200 MeV. (g) π^-p polarization at 100, 180, 280, and 350 MeV. (h) $\pi^-+p\rightarrow\pi^0+n$ polarization at 50, 100, 170, 280, and 350 MeV. (i) $\pi^+p\ B(\theta)$ at 70, 90, 160, 220, and 350 MeV. (j) $\pi^+p\ S(\theta)$ at 70, 90, 160, 220, and 350 MeV. (k) $\pi^-p\ B(\theta)$ at 50, 100, 180, 280, and 350 MeV. (l) $\pi^-p\ S(\theta)$ at 50, 100, 180, 280, and 350 MeV. (m) $\pi^-+p\rightarrow\pi^0+n\ B(\theta)$ at 50, 100, 180, 280, and 350 MeV. (n) $\pi^-+p\rightarrow\pi^0+n\ S(\theta)$ at 50, 100, 180, 280, and 350 MeV.

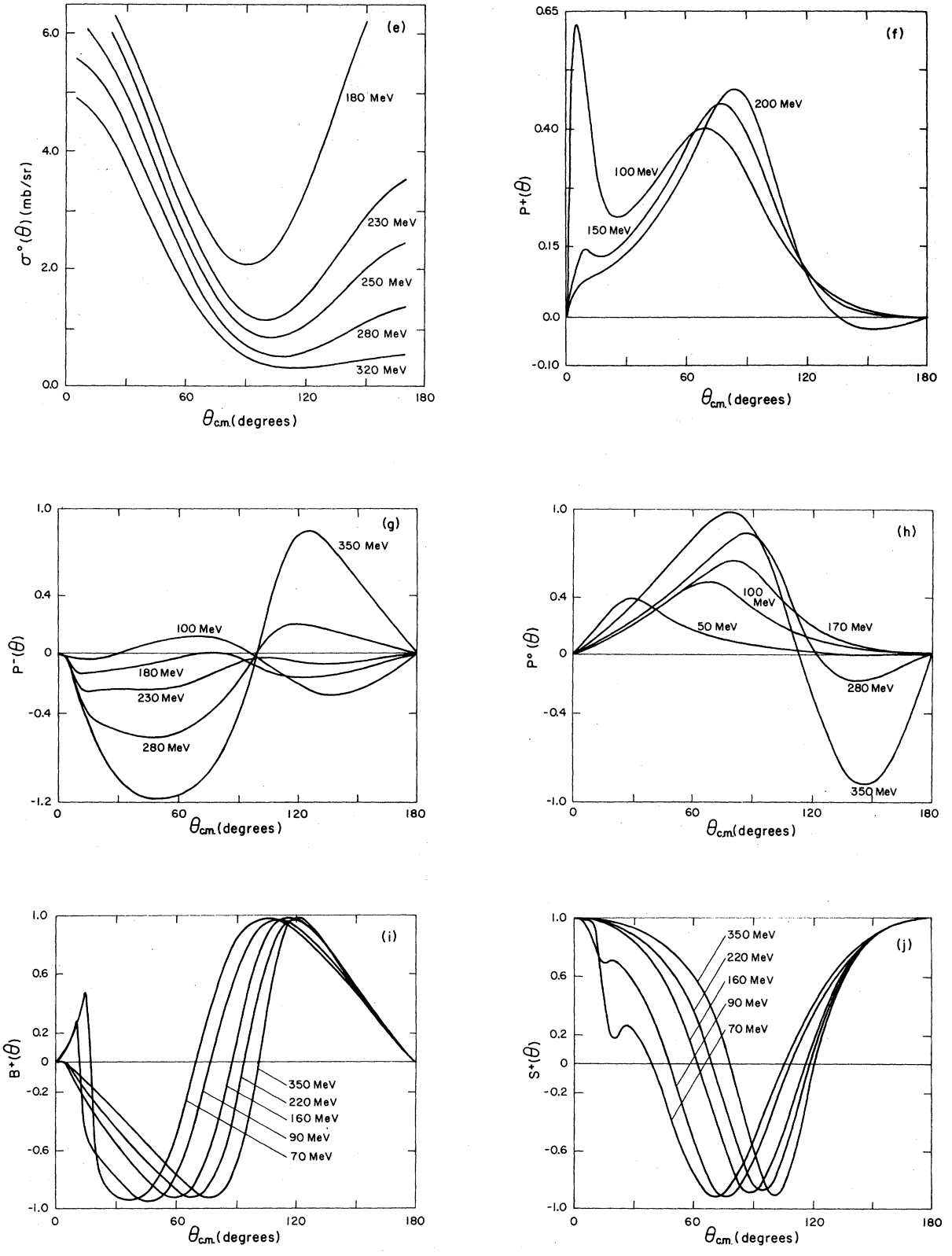

FIG. 5. (*Continued*).

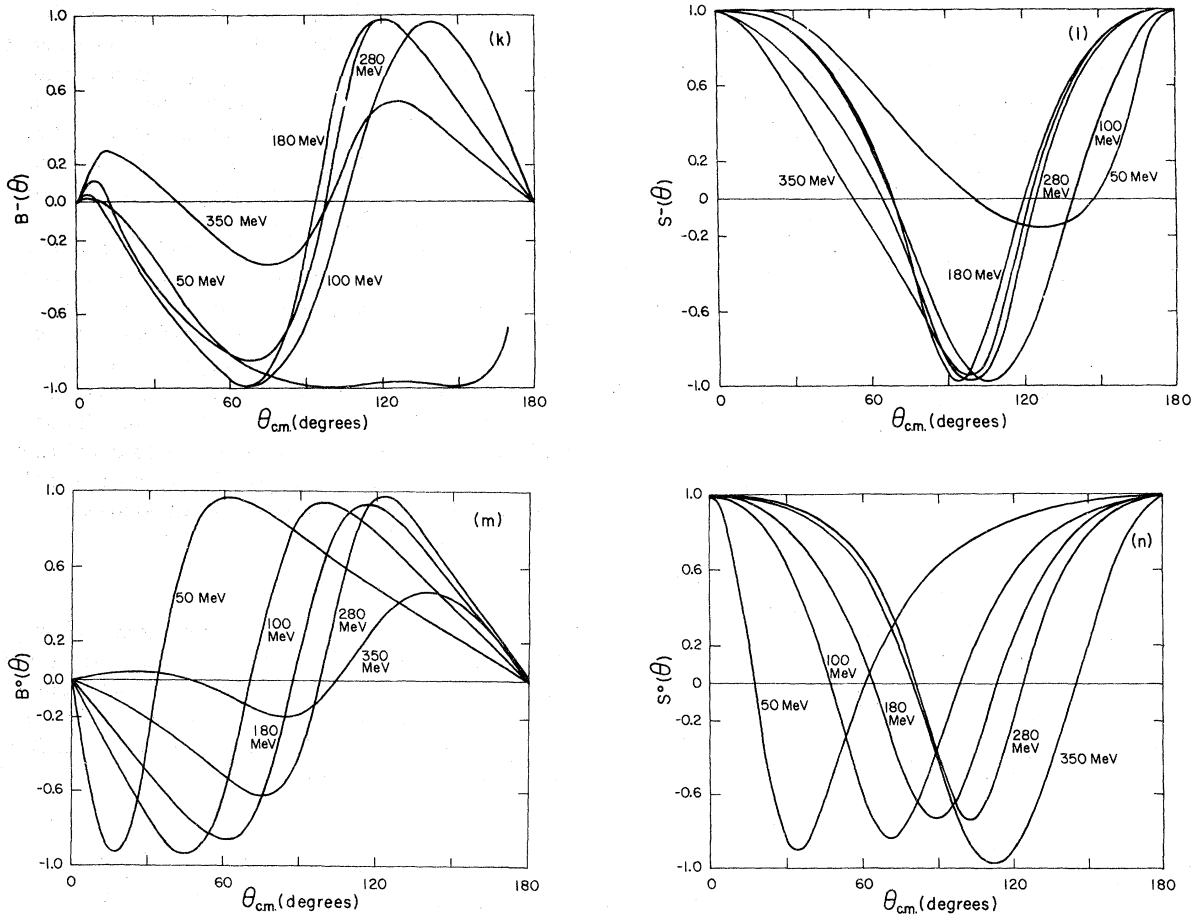

FIG. 5. (*Continued*).

unique determination of the $I=\frac{3}{2}$ S, P, and D waves. The F waves are less well determined but at least exhibit a preferred sign: $F_{37}>0$, $F_{35}\leq 0$. There is no need for theoretical input to determine the peripheral waves; the data alone are adequate and may be used as a constraint on theory.

The relatively small $I=\frac{1}{2}$ component is not well determined by the partial-wave analysis in spite of many recent measurements. There are significant differences for the S_{11} and P_{11} partial waves between the results of this analysis and that of other authors. The high partial waves are especially ill determined in this case.

Overall, however, the phase shifts we have obtained are of sufficient quality to warrant their use, extrapolated off mass shell, as input for pion-nucleus calculations, for critical tests of pion-nucleon dynamical models and in a dispersion theory analysis imposing crossing symmetry and full analyticity in the style of Nielsen and Oades.[3]

The fundamentally new feature of our analysis is the S_{31} charge splitting which we find necessary to include in order to describe the observables most faithfully in the context of our simple parametrization. This effect certainly needs clarification and must be considered before a detailed comparison with dynamical models can be made.

The usual way to fix the energy dependence of the S waves below 100 MeV is by using fixed-t dispersion relations. However, in spite of the sparcity of data below 100 MeV the pion-nucleon phase shifts determined by this data agree to an excellent approximation with those determined by the 0–350 fit. This suggests that by making use of the form 2 parametrization of the amplitude it is possible to extract values for the pion-nucleon scattering lengths. These are defined by the equation

$$C_l^2\rho_l[\cot\delta_{2I,2J}+2\eta h(\eta^2)/C_0^2] = \frac{1}{a_{2I,2J}}+\frac{1}{2}r_{2I,2J}q^2+\cdots, \quad (61)$$

where $a_{2I,2J}$ is the scattering length and $r_{2I,2J}$ is the effective range for scattering from a state of total angular momentum J and isospin I. The parameters for fit A2 then give the following values for the π^+p scattering lengths:

$$\begin{aligned} a_3^+ &= (-0.0990 \pm 0.0013)\hbar/\mu c\,, \\ a_{31} &= (-0.0433 \pm 0.0021)(\hbar/\mu c)^3\,, \\ a_{33}^+ &= (0.2096 \pm 0.0018)(\hbar/\mu c)^3\,. \end{aligned} \tag{62}$$

For B2 we have

$$\begin{aligned} a_1 &= (0.2141 \pm 0.0058)\hbar/\mu c\,, \\ a_3^- &= (-0.1040 \pm 0.0006)\hbar/\mu c\,, \\ a_{11} &= (-0.1316 \pm 0.0027)(\hbar/\mu c)^3\,, \\ a_{13} &= (-0.0564 \pm 0.0154)(\hbar/\mu c)^3\,, \\ a_{33}^- &= (0.2216 \pm 0.0015)(\hbar/\mu c)^3\,. \end{aligned} \tag{63}$$

I-spin breaking thus leads to a difference in scattering lengths of magnitude:

$$\begin{aligned} a_3^+ - a_3^- &= (0.0050 \pm 0.0014)\hbar/\mu c\,, \\ a_{33}^+ - a_{33}^- &= (-0.0120 \pm 0.0023)(\hbar/\mu c)^3\,. \end{aligned} \tag{64}$$

These values for the scattering lengths suggest that the forces causing scattering in the S_{31} state of π^-p are more repulsive than in the case of π^+p. Equation (63) also constitutes a useful way of expressing the magnitude of the I-spin-breaking effect, and it should be a challenge to theorists to account for these numbers.

The T-matrix pole position of the Δ resonance may be determined by analytic continuation of the P_{33} partial-wave amplitude onto the second sheet of the complex energy plane. An alternate, and simpler, method is to parametrize the P_{33} phase shift using the Lichtenberg resonance formula. Using this parametrization, we have obtained precise values for the Δ^{++} and Δ^0 pole positions and residues. This representation also allows us to assign meaningful errors, making a comparison with theoretical calculations possible.

Typically, when new data are added to a data set, no noticeable reduction in the number of existing solutions results. Either the solutions are insensitive to the new data or experimental errors are prohibitively large. Such experiments waste time and resources and can be avoided by careful preexperiment planning. It is most useful to know which experimental observables provide the greatest sensitivity to the differences between existing solutions. Such a sensitivity analysis was first performed by Arndt and Roper[26] on the np scattering problem. A similar analysis may be conducted for the πN problem at energies of experimental interest. Specific results are available on request.

We wish to emphasize that filling gaps in π^+p differential-cross-section data, except perhaps at energies below 100 MeV, will probably not lead to any new insights into πN scattering. Precise charge-exchange differential-cross-section data, especially around the Δ^0 resonance with uniform angular converage, are required to further define the P_{33} mass splitting as well as to clarify S_{31} I-spin breaking. Precise elastic polarization data, especially charge exchange, are required at low energies and in the region of the Δ^0 resonance. Notable for their absence are measurements of the spin-rotation parameters in the first resonance region. This is unfortunate because, supplemented by measurements of $P(\theta)$ and $\sigma(\theta)$ at the same energy and angle, they would constitute a complete data set. This would allow the resolution of ambiguities in single-energy analyses.

ACKNOWLEDGMENTS

This research was supported by a grant from the U. S. Department of Energy. The authors would like to thank M. Blecher for advance communication of his data and Dr. J. B. Cammarata, Dr. Y. N. Goradia, Dr. D. A. Jenkins, and Dr. B. M. K. Nefkens for useful comments.

APPENDIX A: DATA REFERENCES

Total-cross-section references ($1 = \sigma_T^+$, $2 = \sigma_T^-$, $3 = \sigma_T^0$)

T1. H. L. Anderson *et al.*, Phys. Rev. 91, 155 (1953); 1.

T2. H. L. Anderson *et al.*, Phys. Rev. 100, 268 (1955); 1,2.

T3. J. Ashkin *et al.*, Phys. Rev. 101, 1149 (1956); 1,2.

T4. D. V. Bugg *et al.*, Nucl. Phys. B26, 588 (1971); 3.

T5. A. A. Carter *et al.*, Phys. Rev. 168, 1457 (1968); 1.

T6. A. A. Carter *et al.*, Nucl. Phys. B26, 445 (1971); 1,2.

T7. D. Davidson *et al.*, Phys. Rev. D 6, 1199 (1972); 1,2.

T8. D. N. Edwards *et al.*, Proc. Phys. Soc. London 73, 856 (1959); 2.

T9. E. Fermi *et al.*, Phys. Rev. 92, 161 (1953); 2.

T10. M. Glicksman, Phys. Rev. 95, 1045 (1954); 2.

T11. M. Glicksman, Phys. Rev. 94, 1335 (1954); 2.

T12. S. Kellman *et al.*, Phys. Rev. 129, 365 (1963); 2.

T13. U. E. Kruse and R. C. Arndold, Phys. Rev. 116, 1008 (1959); 2.
T14. A. I. Mukhin *et al.*, CERN Report No. CERN SYMP 204, 1956 (unpublished); 1.
T15. D. V. Neagu *et al.*, Stud. Cercet. Fiz. 12, 39 (1961); 1.
T16. J. Orear *et al.*, Phys. Rev. 93, 575 (1954); 1.
T17. H. R. Ruggs and O. T. Vik, Phys. Rev. 129, 2300 (1963); 2.

Differential-cross-section references [4 = $\sigma^+(\theta)$, 5 = $\sigma^-(\theta)$, 6 = $\sigma^0(\theta)$]

D1. H. L. Anderson *et al.*, Phys. Rev. 86, 793 (1952); 6.
D2. H. L. Anderson *et al.*, Phys. Rev. 91, 155 (1953); 4,5.
D3. H. L. Anderson *et al.*, Phys. Rev. 100, 268 (1955); 4,5.
D4. J. Ashkin *et al.*, Phys. Rev. 101, 1149 (1956); 4,5.
D5. J. Ashkin *et al.*, Phys. Rev. 105, 724 (1957); 4,5.
D6. S. W. Barnes *et al.*, Phys. Rev. 117, 226 (1960) and 117, 238 (1960); 4,5.
D7. W. Bayer *et al.*, CERN report, 1975 (unpublished); 6.
D8. P. A. Berardo *et al.*, Phys. Rev. D 6, 756 (1972); 6.
D9. P. Y. Bertin *et al.*, Nucl. Phys. B106, 341 (1976); 4.
D10. M. Blecher (private communication); 4.
D11. D. Bodansky *et al.*, Phys. Rev. 93, 1367 (1954); 4.
D12. P. J. Bussey *et al.*, Nucl. Phys. B58, 363 (1973); 4,5.
D13. Yu. A. Budagov *et al.*, Nucl. Phys. 22, 276 (1961); 5.
D14. J. C. Comiso *et al.*, Phys. Rev. D 12, 738 (1975); 6.
D15. K. M. Crewe *et al.*, UCRL Report No. UCRL-18473, 1968 (unpublished); 4,5.
D16. D. C. Cundy *et al.*, Proc. Phys. Soc. London 85, 275 (1965); 5.
D17. J. Deahl *et al.*, Phys. Rev. 124, 1987 (1961); 5.
D18. R. A. Donald *et al.*, Proc. Phys. Soc. London 87, 445 (1966); 5.
D19. J. Duclos *et al.*, Phys. Lett. 43B, 245 (1973); 6.
D20. D. N. Edwards *et al.*, Proc. Phys. Soc. London 73, 856 (1959); 5.
D21. D. N. Edwards *et al.*, Proc. Phys. Soc. London 92, 602 (1967); 4.
D22. E. Fermi *et al.*, Phys. Rev. 92, 161 (1953); 5.
D23. L. Ferretti *et al.*, Nuovo Cimento 5, 1660 (1957); 4.
D24. L. Ferretti *et al.*, Nuovo Cimento 1, 1238 (1955); 4.
D25. E. C. Fowler *et al.*, Phys. Rev. 36, 1053 (1952); 4.
D26. W. B. Fowler *et al.*, Phys. Rev. 95, 1587 (1954); 4.
D27. R. Gessaroli *et al.*, Nuovo Cimento 5, 1658 (1957); 4.
D28. G. Giacomelli, Phys. Rev. 117, 250 (1960); 4,5.
D29. M. Glicksman, Phys. Rev. 94, 1335 (1954); 5.
D30. M. Glicksman, Phys. Rev. 95, 1045 (1954); 5.
D31. G. Goldhaber *et al.*, Phys. Rev. 89, 1187 (1953); 4.
D32. V. A. Gordeev *et al.*, Yad. Fiz. 24, 1144 (1976) [Sov. J. Nucl. Phys. 24, 599 (1976)]; 4,5.
D33. R. A. Grandey *et al.*, Phys. Rev. 97, 791 (1955); 4.
D34. M. G. Hauser *et al.*, Phys. Lett. B35, 252 (1971); 6.
D35. G. Homa *et al.*, Phys. Rev. 93, 554 (1954); 4.
D36. R. Jenefsky *et al.*, Helv. Phys. Acta 47, 80 (1974); 6.
D37. S. Kellman *et al.*, Phys. Rev. 129, 365 (1963); 5.
D38. D. E. Knapp and K. Kinsey, Phys. Rev. 131, 1822 (1963); 4,5.
D39. U. E. Kruse and R. C. Arnold, Phys. Rev. 116, 1008 (1959); 5.
D40. J. J. Lord and A. B. Weaver, Nuovo Cimento 5, 1238 (1957); 5.
D41. A Loria, Nuovo Cimento 22, 820 (1961); 4.
D42. D. Miller and J. Ring, Phys. Rev. 117, 582 (1960); 4.
D43. A. J. Mukhin *et al.*, CERN Report No. CERN SYMP 204, 1956 (unpublished); 4.
D44. P. M. Ogden *et al.*, Phys. Rev. B 137, 1115 (1965); 4.
D45. J. Orear *et al.*, Phys. Rev. 92, 156 (1953); 5.
D46. J. Orear *et al.*, Phys. Rev. 93, 575 (1954); 4.
D47. J. Orear *et al.*, Phys. Rev. 96, 1417 (1954); 4.
D48. J. P. Perry *et al.*, Phys. Rev. 91, 1289 (1953); 4.
D49. H. R. Rugge and O. T. Vik, Phys. Rev. 129, 2300 (1963); 5.
D50. A. M. Sachs *et al.*, Phys. Rev. 109, 1750 (1958); 4.
D51. H. D. Taft, Phys. Rev. 101, 1116 (1956);

4.
D52. J. Tinlot and A. Roberts, Phys. Rev. 95, 137 (1954); 6.
D53. W. Troka *et al.*, Phys. Rev. 144, 1115 (1966); 4.
D54. I. M. Vasilevski and V. V. Vishnyakov, Zh. Eksp. Teor. Fiz. 38, 441 (1960) [Sov. Phys.—JETP 11, 323 (1960)]; 5.
D55. O. T. Vik *et al.*, Phys. Rev. 129, 2311 (1963): 4.
D56. S. L. Whetstone *et al.*, Phys. Rev. 102, 251 (1956); 4.
D57. V. G. Zinov and S. M. Kerenchenko, Zh. Eksp. Teor. Fiz. 38, 794 (1960) [Sov. Phys.—JETP 11, 794 (1960)]; 5.

Recoil-nucleon polarization data [$7 = P^+(\theta)$, $8 = P^-(\theta)$, $9 = P^0(\theta)$]

P1. J. C. Alder *et al.*, Lett. Nuovo Cimento 23, 381 (1978); 8.
P2. C. Amsler *et al.*, Phys. Lett. B57, 289 (1975); 7.
P3. C. Amsler *et al.*, Lett. Nuovo Cimento 15, 209 (1976); 7.
P4. J. F. Arens *et al.*, Phys. Rev. 167, 1261 (1968); 8.
P5. O. Chamberlain *et al.*, Phys. Lett. 7, 293 (1963); 7.
P6. L. Dubel *et al.*, Helv. Phys. Acta 50, 815 (1977); 7.
P7. J. H. Foote *et al.*, Phys. Rev. 122, 948 (1961); 7.
P8. W. Gorn *et al.*, Bull. Am. Phys. Soc. 12, 469 (1967); 7, 8.
P9. W. Gorn, UCB thesis, LBL Report No. LBL-1320, 1973 (unpublished); 7, 8.
P10. E. L. Grigoriev and N. A. Mitin, Zh. Eksp. Teor. Phys. 37, 413 (1959) [Sov. Phys.—JETP 10, 295 (1960)]; 7.
P11. R. E. Hill *et al.*, Phys. Rev. D 2, 1199 (1970); 9.
P12. J. F. Kunze *et al.*, Phys. Rev. 117, 859 (1960); 8.
P13. I. M. Vasilevsky *et al.*, Phys. Lett. 23, 174 (1966); 8.

APPENDIX B: πN SCATTERING FORMALISM

For convenience and completeness we include in this appendix the conventions we follow for the πN amplitudes and observables. Partial-wave amplitudes are denoted as usual by $L_{2I,2J}$, where L is the orbital angular momentum state, I is the isospin, and $J = l \pm \frac{1}{2}$ is the total angular momentum. The spin decomposition of the scattering amplitude in the c.m. system goes as follows:

spin-nonflip amplitudes

$$f(s,\theta) = \frac{\lambda}{q} \sum_{l=0}^{\infty} [(l+1)T_{l+}(s) + lT_{l-}(s)]P_l(\cos\theta), \tag{B1}$$

spin-flip amplitude

$$g(s,\theta) = \frac{\lambda}{q} \sum_{l=0}^{\infty} [T_{l+}(s) - T_{l-}(s)]P_l^1(\cos\theta), \tag{B2}$$

where θ is the center-of-mass scattering angle, s is the square of the total center-of-mass energy, and P_l and P_l^1 are the ordinary and associated Legendre polynomials. The partial-wave amplitude is written in terms of the nuclear phase shift $\delta_{l\pm}(s)$ and inelasticity $\eta_{l\pm}(s)$ as

$$T_{l\pm}(s) = \frac{1}{2i}\{\eta_{l\pm}(s)\exp[2i\delta_{l\pm}(s)] - 1\}. \tag{B3}$$

The relevant observables may be expressed in terms of the amplitudes as follows:

Differential cross section for unpolarized target

$$d\sigma/d\Omega = |f(s,\theta)|^2 + |g(s,\theta)|^2. \tag{B4}$$

Recoil-proton polarization for unpolarized target

$$P(s,\theta) = -2\,\mathrm{Im}[f^*(s,\theta)g(s,\theta)]\hat{n}(d\sigma/d\Omega), \tag{B5}$$

where $\hat{n} = (\vec{q}\times\vec{q}')/|\vec{q}\times\vec{q}'|$ and $\vec{q}$, $(\vec{q}')$ is the barycentric momentum of the incident (final) pion.

Real part of the forward amplitude

$$\mathrm{Re}f(s,0) = \frac{\lambda}{q} \sum_{l=0}^{\infty} [(l+1)\mathrm{Re}T_{l+}(s) + l\,\mathrm{Re}T_{l-}(s)]. \tag{B6}$$

Total cross section

$$\sigma_T(s) = 4\frac{\pi\lambda^2}{q}\,\mathrm{Im}f(s,0). \tag{B7}$$

Total inelastic cross section

$$\sigma_{\mathrm{in}}(s) = \frac{\pi\lambda^2}{q^2} \sum_{l=0}^{\infty} \{(l+1)[1-\eta_{l+}{}^2(s)] + l[1-\eta_{l-}{}^2(s)]\}. \tag{B8}$$

Spin-rotation parameters

$$A(s,\theta) = \frac{[(|f|^2 - |g|^2)\sin\theta + 2\,\mathrm{Re}(f^*g)\cos\theta]}{d\sigma/d\Omega}, \tag{B9}$$

$$R(s,\theta) = \frac{[-(|f|^2 - |g|^2)\cos\theta + 2\,\mathrm{Re}(f^*g)\sin\theta]}{d\sigma/d\Omega}. \tag{B10}$$

The spin-rotation parameters are constrained by the equation $A^2 + R^2 + P^2 = 1$.

Electromagnetic corrections. Ordinarily the scattering data are not corrected for photon ex-

change. This correction is important near the forward direction and/or at small q. A straightforward calculation of the one photon exchange amplitude for πN scattering gives

$$f_\gamma^{(\pm)}(s,\theta) = \mp \frac{\alpha\lambda}{4W\sin^2(\theta/2)}\,[F_1(s,\theta) - F_2(s,\theta)], \tag{B11}$$

$$g_\gamma^{(\pm)}(s,\theta) = \mp \frac{\alpha\lambda}{4W\sin^2(\theta/2)}\,[G_1(s,\theta) + G_2(s,\theta)], \tag{B12}$$

where

$$\begin{aligned} F_1(s,\theta) &= \frac{W-m}{E-m} + \frac{W+m}{E+m}\cos\theta\,, \\ F_2(s,\theta) &= (\mu_p - 1)\left(\frac{2(W-E)}{m}\sin^2\frac{\theta}{2} + \frac{E-m}{2m}\sin^2\theta\right), \\ G_1(s,\theta) &= \frac{W+m}{E+m}\,, \\ G_2(s,\theta) &= (\mu_p - 1)\left(\frac{2W-E+m}{2m} + \frac{E-m}{2m}\cos\theta\right), \end{aligned} \tag{B13}$$

where E is the proton barycentric energy, $W = s^{1/2}$, and $\mu_p = 2.792$ is the total magnetic moment of the proton. For charge-exchange scattering the electromagnetic amplitudes vanish exactly. In the nonrelativistic limit, Eqs. (B11) and (B12) reduce to

$$f_{\rm nrel}^{(\pm)}(s,\theta) = \pm\frac{\lambda\eta_R}{2qW}\,, \tag{B14}$$

$$g_{\rm nrel}^{(\pm)}(s,\theta) = 0\,, \tag{B15}$$

where

$$\eta_R = \alpha\,\frac{E(W-E)+q^2}{qW} \tag{B16}$$

is the relativistic generalization of the Coulomb parameter. Equations (B14) and (B15) are the first-order approximations to the full nonrelativistic Coulomb amplitudes. This amplitude results from an exact solution to the nonrelativistic Schrödinger equation for Coulomb scattering,

$$f_{\rm Coul}^{(\pm)} = \mp\frac{\lambda\eta}{2qW}\,e^{\mp i\eta\ln\sin^2(\theta/2)}. \tag{B17}$$

For the total Coulomb amplitudes we utilize the Roper prescription[4]

$$f_C^{(\pm)} = f_\gamma^{(\pm)} + f_{\rm Coul}^{(\pm)} - f_{\rm nrel}^{(\pm)}\,, \tag{B18}$$

$$g_C^{(\pm)} = g_\gamma^{(\pm)}\,, \tag{B19}$$

which gives approximately unitary amplitudes correct to all orders of α nonrelativistically and to first order in α relativistically. The above form for the Coulomb amplitudes is quite adequate for the purposes of phase-shift analysis given the present precision and angular range of the data. Some authors, for example, include a modification of Eqs. (B11) and (B12) due to the electromagnetic structure of the pion and proton. It is then necessary to modify the amplitudes by making the substitutions

$$F_{1,2}(s,\theta) = F_{1,2}(s,\theta)\,f_{1,2}^N(K^2)f^\pi(K^2)\,, \tag{B20}$$

$$G_{1,2}(s,\theta) = G_{1,2}(s,\theta)\,f_{1,2}^N(K^2)\,f^\pi(K^2)\,, \tag{B21}$$

where $f_1^N(K^2)$ and $f_2^N(K^2)$ are the Dirac and Pauli form factors of the proton, $f^\pi(K^2)$ is the pion form factor, and K^2 is the invariant four-momentum transfer $K^2 = 4q^2\sin^2(\theta/2)$.

Ordinarily the proton form factors are approximated by the dipole and scaling formulas. However, as has been pointed out by Hammer *et al.*,[57] the dipole and scaling formulas do not give a good statistical fit to the second-generation form-factor data and must be relegated to the history of physics as only crude, first-order parametrizations. Furthermore, the Coulomb amplitudes are largest for small values of K^2 where the form factors differ only negligibly from their point-particle limits. Therefore, we do not expect, and in fact do not find important consequences to result from refinements of Eqs. (B11) and (B12) of the type proposed, for example, by Tromberg *et al.*[22] Only when full Coulomb corrections to obtain the hadronic phases are required are such refinements necessary.

A product S-matrix description of strong and electromagnetic interactions then gives the following equations for the nuclear amplitudes:

$$f_N^{(\pm)}(s,\theta) = f_C^{(\pm)}(s,\theta) + \frac{\lambda}{q}\sum_{l=0}^{\infty} e^{\pm 2i\sigma_l}[(l+1)T_{N,l+}^{(\pm)}(s) + T_{N,l-}^{(\pm)}(s)]P_l(\cos\theta)\,, \tag{B22}$$

$$g_N^{(\pm)}(s,\theta) = \frac{\lambda}{q}\sum_{l=0}^{\infty} e^{\pm 2i\sigma_l}[T_{N,l+}^{(\pm)}(s) - T_{N,l-}^{(\pm)}(s)]P_l^1(\cos\theta)\,. \tag{B23}$$

For charge exchange there is no final-state electromagnetic interaction, so

$$f_N^{(0)}(s,\theta) = \frac{\lambda}{q}\sum_{l=0}^{\infty} e^{-i\sigma_l}[(l+1)T_{N,l+}^{(0)}(s) + lT_{N,l-}^{(0)}]P_l(\cos\theta)\,, \tag{B24}$$

$$g_N^{(0)}(s,\theta)=\frac{\lambda}{q}\sum_{l=0}^{\infty}e^{-i\sigma_l}[T^{(0)}_{N,l+}(s) - T^{(0)}_{N,l-}(s)]P_l(\cos\theta). \tag{B25}$$

Here σ_l is the Coulomb phase shift, defined by

$$\sigma_l=\arg\Gamma(l+1+i\eta). \tag{B26}$$

Since the Coulomb parameter is very small over the energies at which data are available ($\eta=0.2$ at 20 MeV and 0.008 at 350 MeV), the Coulomb phase shifts are small except at very low energies (for $T_L>20$ MeV, $\sigma_l<1^\circ$). These phases may be calculated by making use of the recurrence relation

$$\sigma_l(\eta)=\sigma_0+\sum_{j=1}^{l}\tan^{-1}\left(\frac{\eta}{j}\right), \tag{B27}$$

where to an excellent approximation $\sigma_0\approx-\eta\gamma$, $\gamma=0.5772$.

As discussed in the text, even though we formally permit I-spin violation, we still retain the language of charge independence and write the nuclear amplitudes in terms of (pseudo) isospin-conserving $I=\frac{1}{2}$ and $\frac{3}{2}$ amplitudes:

$$\begin{aligned} T^{(+)}_{N,l\pm}&=T^{(3)}_{l\pm},\\ T^{(-)}_{N,l\pm}&=\tfrac{1}{3}(T^{(3)}_{l\pm}+2T^{(1)}_{l\pm}),\\ T^{(0)}_{N,l\pm}&=\tfrac{1}{3}\sqrt{2}(T^{(3)}_{l\pm}-T^{(1)}_{l\pm}). \end{aligned} \tag{B28}$$

---

*Present address: Areté Associates, P. O. Box 3800, Santa Monica, California 90403.

[1]S. Almehed and C. Lovelace, Nucl. Phys. B40, 157 (1972).
[2]J. R. Carter, D. V. Bugg, and A. A. Carter, Nucl. Phys. B58, 378 (1973).
[3]H. Nielsen and G. C. Oades, Nucl. Phys. B72, 310 (1974).
[4]L. D. Roper, R. M. Wright, and B. T. Feld, Phys. Rev. 138B, 190 (1965).
[5]L. D. Roper and R. M. Wright, Phys. Rev. 138B, 921 (1965).
[6]R. Ayed, Saclay Report No. CEA-N-1921, 1976 (unpublished).
[7]V. S. Zidell, L. D. Roper, and R. A. Arndt, VPI Report No. VPI-SA-1(78), 1978 (unpublished).
[8]D. B. Lichtenberg, Lett. Nuovo Cimento 12, 616 (1975).
[9]A. A. Carter and J. R. Carter, Rutherford Laboratory Report No. RL-73-024, 1973 (unpublished).
[10]T. R. Englemann and R. E. Hendrick, Phys. Rev. D 16, 2891 (1977).
[11]C. Lovelace, S. Almehed, F. Uchiyama, R. Kelly, and V. Henri, LBL Report No. LBL-63, 1973 (unpublished).
[12]E. Pedroni *et al.*, in *Meson-Nuclear Physics—1976*, proceedings of the International Topical Conference, Pittsburgh, edited by P. D. Barnes (AIP, New York, 1976), p. 25.
[13]B. M. K. Nefkens *et al.*, Experiment No. 363, LAMPF proposal, 1977 (unpublished).
[14]B. M. K. Nefkens *et al.*, Experiment No. 120, LAMPF research proposal, 1972 (unpublished).
[15]M. R. Sogard, Phys. Rev. D 9, 1486 (1974).
[16]E. Borie, Karlsruhe Report No. TKP 77-6, 1977 (unpublished).
[17]D. I. Sober *et al.*, Phys. Rev. D 11, 1017 (1975).
[18]D. J. Herndon *et al.*, Phys. Rev. D 11, 3183 (1975).
[19]The exact magnitude of the rescattering, or unitarity, corrections to the isobar model is still an open problem. Decisive results await the elaboration of models incorporating both unitarity and analyticity. In any case, it is to be expected that in our energy range the corrections are very small, making the quasi-two-body final-state treatment quite accurate.
[20]P. A. Berardo *et al.*, Phys. Rev. Lett. 26, 201 (1971).
[21]We prefer to parametrize in terms of E_L rather than P_L, q, or W because it is linearly related to s.
[22]B. Tromberg, S. Waldenstrom, and I. Overbo, Phys. Rev. D 15, 725 (1977).
[23]G. L. Shaw and M. H. Ross, Phys. Rev. 126, 806 (1963).
[24]P. Laurikainen and N. A. Tornqvist, Lett. Nuovo Cimento 7, 237 (1973).
[25]R. Ayed, P. Bareyre, and P. Sondereggen, in Proceedings of the Amsterdam International Conference on Elementary Particles, 1971 (unpublished).
[26]R. A. Arndt and L. D. Roper, Nucl. Phys. B50, 285 (1972).
[27]R. A. Arndt and M. H. MacGreggor, *Methods of Computational Physics* (Academic, New York, 1966), Vol. 6, p. 253.
[28]The data base may actually be pruned in a different way—by eliminating all high-χ^2 data sets rather than individual data points. After reminimization the new fits giving χ^2/datum of one differ from A1 and B1 only in the magnitudes of some of the D and F waves.
[29]G. Rowe, M. Salomon, and R.H. Landau, TRIUMF Report No. TRI-PP-78-1, 1978 (unpublished).
[30]A. Donnachie and J. Hamilton, Phys. Rev. 138B, 678 (1965). We have used the values and errors for the DH phases reported in Ref. 2.
[31]J. W. Alcock and W. M. Cottingham, Nucl. Phys. B41, 141 (1972), and private communications. In our energy range we have access only to values of the positive and negative subtraction parts to the dispersion relations of AC. They are expected to give a good approximation to the real part of the scattering amplitude.
[32]T. Y. Cheng and D. B.Lichtenberg, Phys. Rev. D 7, 2249 (1973).
[33]T. G. Trippe *et al.*, Rev. Mod. Phys. 48, S31 (1976).
[34]J. S. Ball and R. L. Goble, Phys. Rev. D 11, 1171

(1975).
[35]S. S. Vasan, Carnegi-Mellon University Report No. COO-3066-58, 1975 (unpublished).
[36]D. B. Lichtenberg, Lett. Nuovo Cimento 7, 727 (1973).
[37]R. Socolow, Harvard University thesis, 1964 (unpublished).
[38]M. Cini and P. Stichel, University of Bielefeld Report No. Bi-72/09, 1972 (unpublished).
[39]S. Eliezer and P. Singer, Phys. Rev. D 8, 2235 (1973).
[40]S. Ono, Physikalisches Institut Technische Houschule Aachen, report, 1976 (unpublished).
[41]W. Celmaster, Phys. Rev. D 15, 1391 (1977).
[42]N. G. Deshpande *et al.*, Phys. Rev. D 15, 1885 (1977).
[43]D. B. Lichtenberg (unpublished).
[44]B. Tromberg *et al.*, Helv. Phys. Acta 51, 584 (1978).
[45]H. Pilkuhn, Nucl. Phys. B82, 365 (1974).
[46]R. Van Royen and V. F. Weisskopf, Nuovo Cimento 50, 617 (1967).
[47]C. Becchi and G.Morpurgo, Phys. Rev. 149, 1284 (1966).
[48]J. Katz and S. Tatur, Nuovo Cimento 40A, 135 (1977).
[49]V. S. Zidell, R. A. Arndt, and L. D. Roper, Lett. Nuovo Cimento 21, 140 (1978).
[50]J. S. Ball, P. S. Lee, and G. L. Shaw, Phys. Rev. D 7, 2789 (1973).
[51]F. S. Henyey and G. L. Kane, University of Michigan Report No. UM-HE 73-16, 1973 (unpublished).
[52]M. G. Olsson, Nuovo Cimento 40A, 284 (1977).
[53]S. M. Bilenkii and R. M. Ryndin, Yad. Fiz. 4, 646 (1966) [Sov. J. Nucl. Phys. 4, 457 (1967)].
[54]N. W. Dean and P. Lee, Phys. Rev. D 5, 2741 (1972).
[55]R. J. Cence, *Pion-Nucleon Scattering* (Princeton University Press, Princeton, New Jersey, 1969), p. 74.
[56]F. A. Berends and J. C. J. M. Van Reisen, Phys. Lett. 64B, 183 (1976).
[57]C. L. Hammer, T. A. Weber, and V. S. Zidell, Phys. Rev. D 9, 189 (1974).